Comparisons of dual isogenic human iPSC pairs identify functional alterations directly caused by an epilepsy associated *SCN1A* mutation

Authors:

Yunyao Xie[1], Nathan N. Ng[1, #a], Olga S. Safrina[1], Carmen M. Ramos[1], Kevin C. Ess[2], Philip H. Schwartz[3], Martin A. Smith[4], Diane K. O'Dowd[1]*

[1] Department of Developmental and Cell Biology, University of California, Irvine, Irvine, CA

[2] Department of Pediatrics, Vanderbilt University Medical Center, Nashville, TN

[3] Children's Hospital of Orange County Research Institute, Orange, CA.

[4] Department of Anatomy and Neurobiology, University of California, Irvine, Irvine, CA

[#a] Current Address: Stanford University, School of Medicine, Stanford, CA 94305

***Correspondence Address:**

Diane K. O'Dowd

4221 McGaugh Hall, University of California, Irvine

Irvine, CA 92697

Phone: +1 (949) 824-8141

Email: dkodowd@uci.edu

Abstract:

Over 1250 mutations in *SCN1A,* the Nav1.1 voltage-gated sodium channel gene, are associated with seizure disorders including GEFS+. To evaluate how a specific mutation, independent of genetic background, causes seizure activity we generated two pairs of isogenic human iPSC lines by CRISPR/Cas9 gene editing. One pair is a control line from an unaffected sibling, and the mutated control carrying the GEFS+ K1270T *SCN1A* mutation. The second pair is a GEFS+ patient line with the K1270T mutation, and the corrected patient line. By comparing the electrophysiological properties in inhibitory and excitatory iPSC-derived neurons from these pairs, we found the K1270T mutation causes cell type-specific alterations in sodium current density and evoked firing, resulting in hyperactive neural networks. We also identified differences associated with genetic background and interaction between the mutation and genetic background. Comparisons within and between dual pairs of isogenic iPSC-derived neuronal cultures provide a novel platform for evaluating cellular mechanisms underlying a disease phenotype and for developing patient-specific anti-seizure therapies.

Keywords:

Isogenic, induced pluripotent stem cells, neurons, *SCN1A*, genetic epilepsy with febrile seizure plus, electrophysiology, disease modeling

50 **1. Introduction**

51 Genetic epilepsy with febrile seizure plus (GEFS+) is a form of epilepsy with
52 febrile seizures that persists beyond six years of age (Scheffer and Berkovic,
53 1997). The clinical phenotype of GEFS+ is characterized by febrile seizures
54 beginning in infancy that persist beyond 6 years of age and in some cases
55 individuals also experience myoclonic, atonic and/or absence seizures (Miller
56 and Sotero de Menezes, 2014). Mutations in a variety of genes that encode ion
57 channels and neurotransmitter receptors have been identified in individuals
58 with GEFS+ (Baulac et al., 2001; Dibbens et al., 2004; Escayg et al., 2001,
59 2000; Harkin et al., 2002; Sugawara et al., 2001; Wallace et al., 2002, 2001a,
60 2001b, 1998). One hot spot for mutations causing GEFS+ is the *SCN1A* gene
61 which encodes the alpha subunit of the Nav1.1 voltage-gated sodium channel.
62 Approximately 50 missense mutations at locations throughout *SCN1A* are
63 associated with different individuals diagnosed with GEFS+ (Meng et al., 2015).
64 There are also multigenerational families in which individuals with the same
65 *SCN1A* mutation exhibit a broad range of seizure phenotypes (Abou-Khalil et
66 al., 2001; Goldberg-Stern et al., 2014).

67 The heterogeneity of disease phenotypes arising from different mutations
68 in the same gene, and from the same mutation between individuals complicates
69 understanding of the underlying cellular mechanisms. Model systems that aid
70 in mapping the links between individual *SCN1A* mutations and their cellular
71 effects can facilitate development of more effective patient-specific drug
72 therapies. Zebrafish, knock-in *Drosophila* and mouse models have all been
73 important tools in this endeavor (Schutte et al., 2016) but evolutionary distances

74 leading to species-specific mechanisms may lead to failed therapies in patients
75 (Marian, 2011; Maxwell et al., 2014).

76 In recent years, patient-derived induced pluripotent stem cells (iPSCs) that
77 can be differentiated into neurons have emerged as a new model to explore
78 how epilepsy-associated *SCN1A* mutations affect activity and sodium channel
79 properties in human neurons. These studies have focused on mutations
80 associated with Dravet syndrome (DS), a form of epilepsy that is typically more
81 severe than GEFS+. Previous studies in iPSC-derived neurons have shown
82 that nonsense R1645X, and missense S1328P and Q1923R mutations in
83 *SCN1A* associated with DS confer impaired excitability and reduced sodium
84 current density in inhibitory neurons, giving rise to hyperactivity in neural
85 networks (Higurashi et al., 2013; Liu et al., 2016; Sun et al., 2016). However,
86 examination of the DS-associated *SCN1A* missense mutations, Q1923R and
87 F1415I, revealed increased excitability and increased sodium current
88 amplitudes in excitatory neurons (Jiao et al., 2013). Further, the IVS14+3A>T
89 mutation which causes truncation of DIIS2 and S3 of Nav1.1 affects both
90 excitatory and inhibitory neurons (Liu et al., 2013).

91 In addition to alterations caused by discrete mutations, differences in
92 genetic background represent a major source of variability that complicates
93 interpretation of any experimental findings as they can influence phenotypic
94 differences (Liang and Zhang, 2013; Vitale et al., 2012). Evaluation of a large
95 cohort of control and patient iPSC lines can help assess the contribution of
96 mutations to disease phenotypes (Sandoe and Eggan, 2013). This is
97 problematic when evaluating potential changes in electrophysiological

98 properties that require examination at the single cell level in multiple cells from
99 a large number of cell lines. However, a more direct way to examine the effect
100 of a mutation independent of genetic background is to compare the cellular
101 changes caused by a single mutation in isogenic pairs of control and mutant
102 iPSC lines (Bassett, 2017; Chen et al., 2014; Liu et al., 2016; Sandoe and
103 Eggan, 2013; Smith et al., 2018). A recent study of the DS-associated *SCN1A*
104 Q1923R mutation used transcription activator-like effector nucleases (TALENs)
105 to generate an isogenic corrected line by removing the *SCN1A* mutation (Liu et
106 al., 2016). Comparison of the isogenic corrected versus the patient line
107 revealed a decrease in sodium current density in inhibitory neurons in the
108 patient line. Comparison of the isogenic corrected line with a control line from
109 a different genetic background revealed additional alterations in the voltage
110 dependence of sodium current activation and action potential (AP) threshold
111 suggesting these might be associated with the genetic background of the
112 patient. An isogenic mutant line in which the mutation had been introduced into
113 the control would have been able to distinguish whether this was due to genetic
114 background or interaction between the mutation and the genetic background.
115 The current study focuses on assessing the contribution of the autosomal
116 dominant *SCN1A* K1270T mutation identified in a GEFS+ family to the etiology
117 of the disease (Abou-Khalil et al., 2001). Two isogenic pairs of iPSC lines
118 generated by CRISPR/Cas 9 gene editing were used: 1a) control (unaffected
119 sibling), 1b) mutated control homozygous for the K1270T mutation, and 2a)
120 patient heterozygous for the K1270T *SCN1A* mutation (GEFS+ sibling), 2b)
121 corrected patient. All 4 iPSC lines in the two isogenic pairs can be differentiated

122 into functional mixed neuronal cultures containing both GABAergic and
123 glutamatergic neurons that expressed Nav1.1. Comparison of
124 electrophysiological properties of neurons within and between pairs identified
125 mutation-dependent alterations independent of genetic background. There
126 were also differences found to be associated with the genetic background and
127 others the result of interactions between the mutation and the background.
128 Such CRISPR/Cas9-based disease modeling strategy with dual isogenic pairs
129 of iPSC-derived neurons represents a promising platform for studying the
130 causality of mutations related to genetic diseases and developing patient-
131 specific therapies based on disease mechanisms.
132

133 **2. Methods**

134 *2.1 Preparation and maintenance of hiPSCs*

135 Skin fibroblasts were collected from two male siblings of the GEFS+ family
136 by Kevin Ess (Vanderbilt University Medical Center) after obtaining informed
137 consent using IRB approved protocol #080369. The control fibroblast donor had
138 no known clinical diagnoses; the patient sibling had four febrile seizures
139 beginning at 6 months of age and four generalized atypical absence seizures
140 since the age of two (Abou-Khalil et al., 2001). Age at time of biopsy the control
141 sibling was 23 years and the patient sibling was 21 years old.

142 Skin fibroblasts were reprogrammed into iPSCs using nonintegrating
143 Sendai virus by the Schwartz laboratory as published (Stover et al., 2013). Two
144 human iPSC lines were generated, SC210.12-SF6-2I3.M11S8 (control) and
145 SC215.19-SF4-2I8.M10S6 (patient). iPSCs were maintained in feeder-free

146 conditions following published protocols (Stover et al., 2013; Stover and
147 Schwartz, 2011).
148
149 *2.2 CRISPR/Cas9 editing on iPSCs derived from two siblings*
150 To generate a mutated control line, the K1270T mutation was knocked into
151 an iPSC line generated from the unaffected sibling (SC210.12-SF6-2I3-M11S8-
152 S4-S6-S2). The 20-nt guide RNA (sgRNA) 5'-CTTCTAAAATGGGTGGCATA-3'
153 was designed using the CRISPR design tool (http://crispr.mit.edu) from the
154 Zhang laboratory and cloned into plasmid pSpCas9(BB)-2A-Puro (Px459) V2.0
155 (Addgene, 62988). Plasmid constructs were purified with the Endo-free Plasmid
156 Maxiprep kit (Qiagen). The 140-nt repair template ssODN1 5'-
157 GATTAAGACGATGTTGGAATATGCTGACAAGGTTTTCACTTACATTTTCATT
158 CTGGAAATGCTTCTAACATGGGTGGCATATGGATATCAAACATATTTCACC
159 AATGCCTGGTGTTGGCTGGACTTCTTAATTGTTGATG-3' (Integrated DNA
160 Technologies) was designed with two homologous arms flanking the Cas9
161 cleavage site, the threonine codon (ACA) at the mutation site and an addition
162 of a silent EcoRV mutation.
163 To generate a corrected patient line, the mutation was removed from a
164 patient iPSC line (SC215.19-SF4-2I8.M10S6-S2-S2). sgRNA (5'-CTTCTAAC
165 ATGGGTGGCATA-3') complementary to the target sequence of mutated allele
166 was cloned into the same plasmid. The 140-nt repair template ssODN2 5'-
167 GATTAAGACGATGTTGGAATATGCTGACAAGGTTTTCACTTACATTTTCATT
168 CTGGAAATGCTTCTAAAATGGGTGGCATATGGCTATCAAACATATTTCACC
169 AATGCCTGGTGTTGGCTGGACTTCTTAATTGTTGATG-3' (Integrated DNA

170 Technologies) was similar to ssODN1 but with the lysine codon at the mutation
171 site (AAA) and without EcoRV silent mutation. 8 x 10^5 cells were co-transfected
172 with 3 μg plasmid-sgRNA construct and ssODN (0.6 μM final concentration)
173 with Amaxa Human Stem Cell Nucleofector Kit 1 (Lonza) and program A-023
174 for the Amaxa Nucleofector Device II. To obtain low seeding density, the
175 transfected cell suspension was diluted in a 1:6 - 1:8 ratio and plated into
176 Matrigel (BD Biosciences)-coated wells of 6-well plates. 24 hours post-
177 transfection, cells were treated with 2 μg/ml puromycin (Sigma-Aldrich) in
178 StemPro complete media (Stover and Schwartz, 2011) containing 0.58 μl/ml
179 SMC4 (Corning). 48 hours post-transfection, cells were switched to normal
180 StemPro complete media containing 0.58 μl/ml SMC4. Continued maintenance
181 required media that included 50% conditioned media from 70-90%-confluent
182 unedited iPSC cultures and 50% StemPro complete media with 55 μM β-
183 mercaptoethanol (Invitrogen), 1×StemPro (Invitrogen), 20 ng/ml bFGF
184 (Stemgent) and 0.58 μl/ml SMC4. 6-8 days post-nucleofection, isolated iPSC
185 colonies with 20-30 cells were formed, picked manually using customized glass
186 hooks, and transferred to single wells in 96- or 48-well plates with pre-wet 20 μl
187 barrier micropipette tips. StemPro complete media supplemented with 0.58
188 μl/ml SMC4 was used for daily feeding. At 100% confluence, clones were split
189 with pre-warmed 62 μl (96-well plate) or 125 μl (48-well plate) of Accutase
190 (Millipore) in a 1:2 ratio. Cells were eventually expanded into two wells in a 48-
191 well plate to be used for freezing as well as sequencing and/or restriction
192 digestion, respectively. All media for feeding and splitting were prepared
193 immediately prior to use and equilibrated at 37°C and 5% CO_2.

194 A protocol for freezing iPSCs in low density was modified from Stover *et al*
195 (Stover and Schwartz, 2011). Cells at 100% confluence were cryopreserved
196 with pre-chilled freezing medium containing 40% conditioned medium from 70-
197 90% confluent culture, 40% StemPro complete medium, 10% DMSO (Sigma-
198 Aldrich), 10% bovine serum albumin (25% BSA, Gibco) with addition of 0.58
199 μl/ml SMC4. To increase viability of cells during defrosting, clones from 48-well
200 plates were frozen with 50-250 μl of freezing medium depending on the size of
201 pellets after centrifugation and were stored in 1.2 ml cryo-vials at -80°C.
202 Genomic DNA was extracted with 10-13 μl of QuickExtract DNA Extraction
203 Solution (Epicentre). Fragments around the intended mutation sites were
204 amplified by PCR in 50 μl reactions with Taq DNA polymerase (Invitrogen),
205 forward primer 5'- CTACCATAGATTCCATCCCCCAA -3' and reverse primer 5'-
206 TTCCACCAATAGTCTTTCCCCTG -3'. PCR products were confirmed by gel
207 electrophoresis and purified with MinElute PCR Purification Kit (Qiagen) prior
208 to sequencing (Retrogen). MacVector software was used to analyze
209 sequencing data.
210 Additionally, a subset of mutated control clones was subject to restriction
211 digestion by EcoRV prior to sequencing analysis. As we observed the absence
212 of EcoRV mutation in some of the positive clones with K1270T mutation, direct
213 sequencing was used to screen the remaining clones.
214 The top five potential off-target sites from CRISPR/Cas9 editing as
215 identified by the CRISPR design tool (http://crispr.mit.edu) from the Zhang
216 laboratory, were *SCN7A*, *FLII*, *SCN2A*, *SCN3A* and *SCN9A*. To determine if
217 any of these were also affected by the editing in the mutated control or the

218 patient corrected line, primers were used to interrogate the relevant region of
219 homology in each gene. PCR conditions were 94 °C, 45 s, 60 °C, 33 s and 72 °C,
220 55 s for 35 cycles.

221 To evaluate the expression level of off targets, mRNA was extracted from
222 neuronal cultures of the mutated control line. cDNA was synthesized following
223 the instructions of TRIzol (Thermo Fisher) and SuperScript™ III First-Strand
224 Synthesis SuperMix for qRT-PCR kit (Thermo Fisher), followed by nested PCR.
225 Expression of the off-target gene was compared to *SCN1A* and normalized to
226 *ACTB*. Nested PCR conditions were 94 °C, 45 s, 60 °C, 33 s and 72 °C, 60 s
227 for 35 cycles for all primers. Primers for sequencing and nested PCR are in
228 Supplementary Table 1.

229 All 4 iPSC lines were karyotyped and cell lines at low passage were
230 expanded for cryopreservation. When samples were thawed for expansion and
231 use in differentiation studies, the *SCN1A* gene was sequenced every 20-30
232 passages. Research was approved by hSCRO (#2011-1023) and IBC protocols
233 (#2011-1377).

234

235 *2.3 Differentiation of two pairs of isogenic iPSCs into neurons*

236 Two pairs of isogenic iPSCs (4 lines total) within 40 passages of the original
237 generation were patterned into neurons as described (Xie et al., 2018). Neural
238 progenitor cells derived from iPSCs were plated on top of 50-70% confluent
239 mouse astroglial feeder layers that were prepared following a published
240 protocol (Schutte et al., 2018).

241 At D17 post-plating, excitatory and inhibitory neurons were labeled by

242 transfection with CaMKII-eGFP (Addgene, 50469) and GAD1-mCherry
243 (Genecopoeia, HPRM15652-PM02) plasmids in Opti-MEM (Gibco) and DNA-
244 in (MTI-GlobalStem) or ViaFect (Promega) reagents.
245
246 *2.4 Immunostaining and imaging*
247 To evaluate the expression of pluripotency markers, iPSCs were plated
248 onto glass coverslips coated with Matrigel diluted 1:30 in DMEM/F-12 +
249 Glutamax (Gibco). iPSCs were maintained using StemPro medium (section
250 2.2). When grown to ~70% confluence, coverslips were fixed and stained as
251 described (Xie et al., 2018). Primary antibodies OCT-3/4 (1:100; Santa Cruz
252 Biotechnology, sc-5279), SOX2 (1:100; Santa Cruz Biotechnology, sc-365823)
253 and NANOG (1:50; Santa Cruz Biotechnology, sc-293121) were used to
254 characterize the pluripotency of the iPSCs. 4',6-diamidino-2-phenylindole
255 (DAPI; Life Technologies) staining was added to visualize nuclei.
256 iPSC-derived neurons were stained with antibodies of βIII-tubulin (1:1000;
257 Sigma-Aldrich, T8660) and GABA (1:4000; Sigma-Aldrich, A2052) to assess
258 the proportion of GABAergic neurons. Neurons were identified by morphology,
259 expression of βIII-tubulin in the cell bodies and neuronal processes, and
260 nuclear localization of DAPI. Identities of neurons labeled by GAD1-mCherry
261 and CaMKII-eGFP plasmids were verified by staining with antibodies of GABA
262 and CaMKII (1:800; Cell Signaling Technology, 3362) respectively. Expression
263 of Nav1.1 was examined in $GABA^+$ (1:100; Aldrich-Sigma, A0310) and CaMKII-
264 $eGFP^+$ cells by staining with anti-Nav1.1 antibody (1:800; Alomone Labs, ASC-
265 001).

266 Images were taken by a Zeiss M2 Imager fluorescence microscope and
267 processed using the supplied Zen software.
268
269 *2.5 Whole-cell recording*
270 Whole-cell recordings were obtained from iPSC-derived inhibitory and
271 excitatory neurons at D21-23 post-plating at room temperature. This time period
272 was selected based on studies in two control cell lines demonstrating that a
273 high percentage of neurons were functionally active by this age (Xie et al.,
274 2018). Patch pipettes were pulled from unpolished borosilicate glass (VWR
275 International) by PC-10 pipette puller (Narishige). Open tip resistance was 6-8
276 MΩ. External solution contained (in mM): 120 NaCl, 5.4 KCl, 0.8 $MgCl_2$, 1.8
277 $CaCl_2$, 15 glucose, 20 HEPES, with pH at 7.2-7.4. Osmolality was adjusted to
278 290 - 295 mOsm. Internal solution contained (in mM): 120 potassium gluconate,
279 20 NaCl, 0.1 $CaCl_2$, 2 $MgCl_2$, 1.1 EGTA, 10 HEPES, 4.5 Na_2ATP with pH at 7.2.
280 Osmolality was around 280 - 283 mOsm. Voltages were corrected for a 5 mV
281 junction potential. To record evoked action potentials, membrane potential was
282 held at -75 mV by injecting sub-threshold currents and cells were depolarized
283 by a series of current injections.
284 Excitatory and inhibitory postsynaptic currents (EPSCs and IPSCs) were
285 separated at reversal potentials (-49 mV and -2 mV) with a gap-free protocol
286 under voltage clamp. Recordings of spontaneous PSCs (sPSCs) were
287 performed with the standard external solution and a cesium gluconate internal
288 solution containing (in mM): 130 Cs^+ gluconate, 0.2 EGTA, 2 $MgCl_2$, 6 CsCl, 10
289 HEPES, 2.5 adenosine 5' triphosphate sodium salt, 0.5 guanosine 5'

290 triphosphate sodium and 10 disodium phosphocreatine. Voltages were
291 corrected for a 7 mV junction potential. Miniature postsynaptic currents
292 (mPSCs) were recorded in external solution containing 1 μM TTX (tetrodotoxin;
293 Alomones Labs).

294 Isolated sodium currents were recorded with external solution containing
295 (in mM): 120 NaCl, 5.4 KCl, 0.8 $CoCl_2$, 15 glucose, 20 HEPES, 2.5
296 tetraethylammonium and 1.0 4-aminopyridine. The same cesium gluconate
297 internal solution for PSC recording was used for sodium current recording.
298 Voltages were corrected for a 10 mV junction potential. P/N leak subtraction
299 was turned on. The voltage dependence of activation was determined with a
300 step protocol. Cell membrane potential was increased from a holding potential
301 of -100 mV to a range of potentials between -100 mV and 30 mV for 45 s with
302 a step interval of 5 or 10 mV. Currents recorded at the shared voltage steps
303 were included for current density analysis and G-V graph plotting. Peak
304 transient currents were plotted against holding potentials and fit with the
305 following equation:

306 $$\mathrm{I} = \frac{(V-Vrev)\times Gmax}{1+\exp\left(-\frac{V-Vhalf}{k}\right)} \qquad (1)$$

307 where I is the peak current amplitude, V is the holding potential of each pulse,
308 V_{rev} is the reversal potential, G_{max} is the maximal conductance, V_{half} is the
309 voltage with 50% channels activated, and k is the slope. Current data in 5 mV
310 and 10 mV step intervals were used for fitting. Conductance was calculated
311 with the following equation:

312 $$\mathrm{G} = \frac{I}{V-Vrev} \qquad (2)$$

313 where G is conductance, and I, V, V_{rev} were as described in equation (1).

The voltage dependence of steady-state inactivation was analyzed with a two-step protocol. It began with a holding potential of -100 mV. Next the conditioning pulse was increased through a series of voltage steps from -100 mV to 30 mV for 90 ms with a step interval of 5 or 10 mV. Currents recorded at the shared voltage steps were included for G-V graph plotting. A test pulse at -10 mV for 90 ms was immediately applied and followed by a holding potential of -100 mV. The peak current amplitude during test pulses were normalized to that during the first test pulse and then plotted against the holding potential of the conditioning pulse. The I-V curves were fitted to the following equation:

$$\mathrm{I} = \frac{1}{1+exp\frac{V-Vhalf}{k}} \qquad (3)$$

where I is the normalized peak current amplitude during the test pulses, V_{half} is the voltage with 50% channels inactivated, and k is the slope. Current data in 5 mV and 10 mV step intervals were used for fitting.

The recovery from steady-state inactivation was determined using a second two-pulse protocol. Following a holding potential of -100 mV for 27 ms, two test pulses at -10 mV for 90 ms were separated by a time interval with a range of 1-10 ms with an increment of 1 ms in the first protocol, and 10-50 ms with an increment of 5 ms in the subsequent protocol. Peak current amplitude from the second pulse was normalized to the average current amplitude from the first pulse to calculate the fractional recovery. The data of recovery were fitted using the following equation:

$$\mathrm{I} = \mathrm{A} \times \exp\left(-\frac{t}{\tau}\right) + B \qquad (4)$$

where I is the normalized current amplitude, A is the relative percentage of recovered currents, t is the time interval, and τ is the time constant of recovery.

338 Electrophysiological data were collected with a List EPC7 amplifier and a
339 Digidata 1320A D-A converter (Axon Instruments), or a MultiClamp 700B
340 amplifier and a Digidata 1440A D-A converter (Axon Instruments). Recordings
341 were obtained by pClamp8 or pClamp10 (Axon Instruments) software with a
342 Bessel filter at 2 kHz and a low-pass filter at 10 kHz.
343
344 *2.6 Data Analysis and Statistics*
345 Counting from fluorescent micrographs was conducted in a blinded fashion
346 with respect to cell line. For each coverslip, at least 3 fields with evenly
347 distributed cells observed via DIC were chosen for counting. 3 coverslips each
348 from individual plating of an iPSC cell line were included for counting the
349 number of cells expressing pluripotency markers.
350 Electrophysiological data were analyzed using Clampfit 10.6 (Molecular
351 Devices). Cells that were included in electrophysiological analyses had a leak
352 current amplitude smaller than 50 pA at a holding potential of -75 mV. Evoked
353 action potentials (APs) recorded under current clamp were included if they had
354 a stable baseline at -65 ~ -85 mV with sub-threshold current injection, a peak
355 amplitude ≥ -5 mV on the first AP and ≥ -15 mV in subsequent APs within the
356 train. AP events were excluded if the maximum firing frequency deviated from
357 mean by more than ± 2SD. Rheobase data were excluded if the resting
358 membrane potentials (RMP) were more depolarized than -35 mV. AP properties
359 were examined in the first AP at rheobase that first elicited AP firing. AP
360 threshold was identified as the first derivative of the membrane potential (dV/dt)
361 5% or higher than the peak rate of change. AP amplitude was defined as the

362 change of membrane potential from the threshold to the peak. AP amplitude
363 and half-width data were not included if the cell did not fire evoked AP. PSCs
364 recorded under voltage-clamp were analyzed using Mini Analysis 6.0.7
365 (Synaptosoft). PSCs were identified as events with an amplitude ≥ 5 pA (2×
366 RMS noise of 2.5 pA) and were then manually verified individually. To calculate
367 the (E-I)/(E+I) index, the absolute values of amplitude or charge transfer of
368 EPSCs and IPSCs were used for E and I respectively. Cells were excluded from
369 sodium current analysis if their current density in the range of -10 - 40mV was
370 2SD beyond the mean.

371 Electrophysiological data are presented with n = number of recorded cells
372 and the number of individual platings shown in parentheses. All data were
373 analyzed with D'Agostino-Pearson normality test. Statistical tests were selected
374 based on the normality test results and performed in Prism 7.0.2 (GraphPad
375 Software). Figures were generated using DeltaGraph 7.1 (Red Rock Software).
376

377 **3. Results**

378 *3.1 Two pairs of isogenic iPSCs generated by CRISPR/Cas9 editing*

379 The autosomal dominant K1270T *SCN1A* mutation identified in a GEFS+
380 family results in a lysine-to-threonine conversion in the second transmembrane
381 segment of the third homologous domain in the α subunit of the human Nav1.1
382 protein (Abou-Khalil et al., 2001) (Figure 1A). Skin fibroblasts were collected
383 from two male siblings (an unaffected control and a GEFS+ patient) and both
384 were reprogrammed into iPSC lines using the nonintegrating Sendai virus
385 (Figure 1B). To examine the contribution of the K1270T mutation to disease

386 phenotypes, two pairs of isogenic lines were included in this study. In the first
387 pair, the GEFS+ K1270T mutation (c.4227A>C) was knocked into the
388 unaffected sibling derived control line using CRISPR/Cas9. For the second
389 isogenic pair, the K1270T mutation in the patient line was corrected
390 (c.4227C>A; Figure 1C). The mutated control clone with desired sequence was
391 homozygous, likely the result of the short distance (9 bp) between the Cas9 cut
392 site and the K1270T mutation locus (Paquet et al., 2016).

393 Sequencing of DNAs from the iPSC lines in the 2 isogenic pairs confirmed
394 that the control line did not have the mutation at site 1270 ($SCN1A^{+/+}$). The
395 mutated control was homozygous for the mutation ($SCN1A^{KT/KT}$) based on
396 sequencing and this was further confirmed by the presence of the silent EcoRV
397 mutation from the repair template in only one allele, demonstrating that the
398 editing process did not also result in loss of one allele and therefore, a
399 hemizygous clone. The patient line was confirmed to be heterozygous for the
400 mutation ($SCN1A^{KT/+}$) and the mutation was absent in the corrected patient
401 lines ($SCN1A^{+/+}$; Figure 1D). The engineered homozygous mutated control
402 provides a unique opportunity to evaluate its cellular defects since two copies
403 of *SCN1A* mutations are usually lethal to organisms *in vivo* (Martin et al., 2010;
404 Yu et al., 2006).

405 Karyotypes of four iPSC lines were verified normal with 46, XY
406 chromosomes (Figure 1E). Pluripotency of each of the 4 cell lines was
407 confirmed by staining for expression of OCT-3/4, SOX2 and NANOG (Yu et al.,
408 2007) (Figure 1F). The top five potential off-target sites for mutations were
409 evaluated, including *SCN7A*, *FLII*, *SCN2A*, *SCN3A* and *SCN9A*

410 (Supplementary Figure 1A). There were no off-target mutations in candidate
411 genes in the corrected patient line. In the homozygous mutated control line,
412 there was a mutation only in *SCN7A*, in addition to the K1270T knock-in
413 mutation. Since *SCN7A* encodes a non-voltage-gated, TTX-insensitive Na_x
414 sodium channel, it is unlikely to affect evaluation of sodium currents and firing
415 properties that are both completely eliminated by addition of TTX to the
416 recording solution (Supplementary Figure 1C). In addition, this gene is
417 expressed in astrocytes, and neurons in circumventricular organs (Gautron et
418 al., 1992; Watanabe et al., 2000) and there is no evidence that this gene is
419 expressed in our iPSC-derived neurons based on nested PCR reactions that
420 resulted in clear amplification of *SCN1A* transcripts with undetectable levels of
421 *SCN7A* (Supplemental Figure 1C).
422

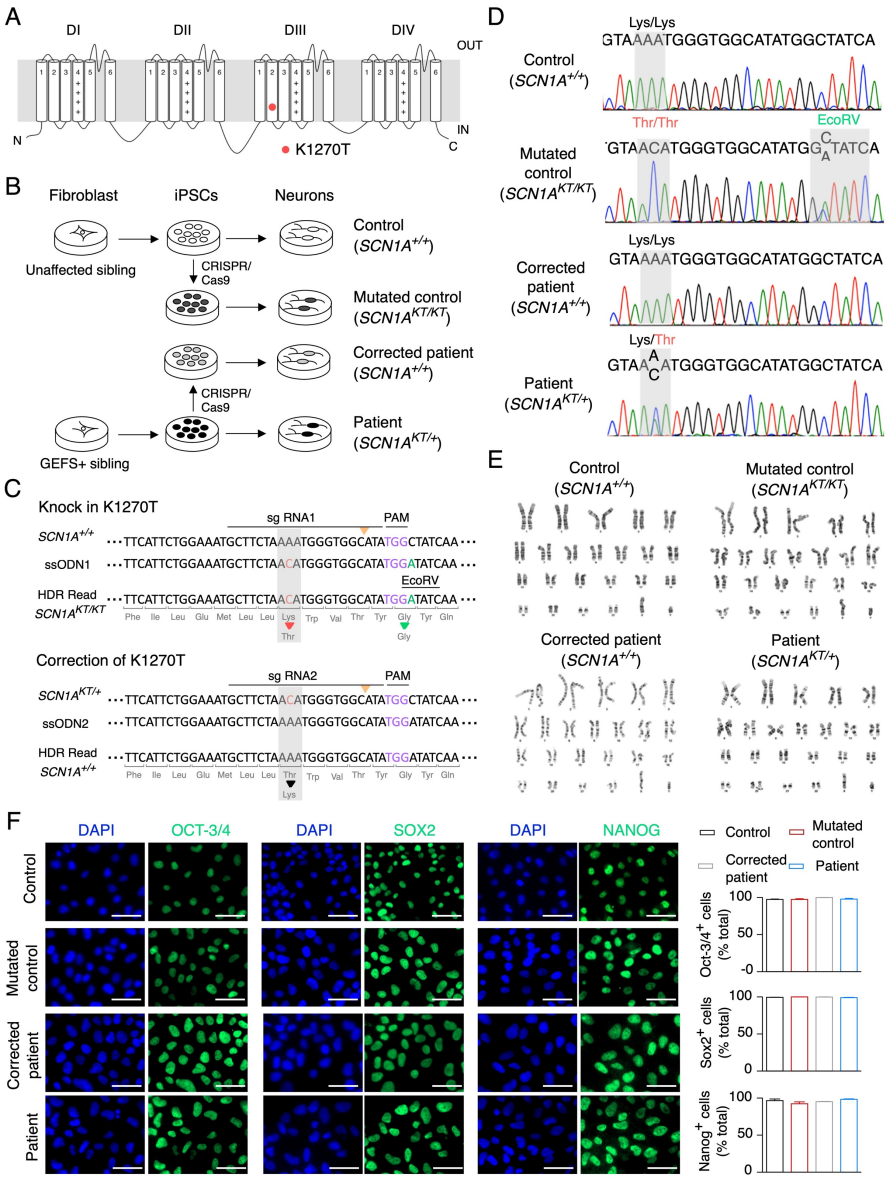

Figure 1. Isogenic pairs of iPSCs generated by CRISPR/Cas9 editing. (A) The K1270T mutation is located in the second transmembrane segment of the third homologous domain of Nav1.1 alpha subunit. (B) CRISPR/Cas9 editing was used to generate two isogenic pairs from iPSCs derived from two siblings in the GEFS+ family (control and patient) followed by differentiation into functional neurons. (C) Scheme of CRISPR/Cas9 editing design. Additional silent mutation introduced by ssODN1 resulted in an EcoRV restriction site for clone screening when knocking in the K1270T mutation. (D) Sequencing of two isogenic iPSC pairs confirmed the absence and the presence of the mutation. (E) All four lines had normal karyotypes (46, XY). (F) iPSCs of two isogenic pairs were stained with nuclei marker DAPI and pluripotency markers OCT-3/4, SOX2 and NANOG individually. The percentage of cells positive for each of the pluripotency markers was not significantly different between the 4 lines ($p = 0.1$, 0.06 and 0.2 for OCT-3/4, SOX2 and NANOG respectively, one-way ANOVA). Scale bar represents 50 μm. Data represented as mean + s.e.m. Data represent counts from three fields in three coverslips from three platings for each genotype.

3.2 iPSC-derived neuronal cultures contain both inhibitory and excitatory neurons

425 We previously optimized a direct differentiation protocol that gives rise to
426 neuronal cultures containing excitatory and inhibitory neurons (Schutte et al.,
427 2018; Xie et al., 2018). With this protocol, iPSCs from both isogenic pairs were
428 differentiated into neural progenitors followed by plating onto astroglial feeder
429 layers for neuronal differentiation. To evaluate the morphology of neurons and
430 quantify the proportion of inhibitory GABAergic and excitatory glutamatergic
431 neurons in the cultures derived from the four iPSC lines, cultures were fixed at
432 D21-24 post plating and stained with anti-βIII-tubulin and anti-GABA or anti-
433 CaMKII antibodies. Cultures from all lines stained βIII-tubulin positive cells with
434 elongated branched neurites (Figure 2A). GABAergic and glutamatergic
435 neurons comprised 30-40% and ~50% of the total neuronal population
436 respectively, with no significance between genotypes (Figure 2B, $p = 0.1$, one-
437 way ANOVA for GABAergic neurons and $p = 0.6$, Kruskal-Wallis test for
438 glutamatergic neurons).

439 In order to identify inhibitory and excitatory neurons during live recording,
440 cells were transiently transfected with GAD1-mCherry and CaMKII-eGFP
441 plasmids at D17 post plating. Visualization of the cultures with fluorescent
442 illumination at D21-24 post plating was used to identify and record from
443 mCherry expressing GAD1-positive inhibitory neurons and eGFP expressing
444 CaMKII-positive excitatory neurons (white arrows, Figure 2C). The plasmid
445 labeling strategy accurately identified GABAergic and glutamatergic neurons
446 based on the colocalization of anti-GABA staining in 90.05% ± 3.26% of GAD1-
447 mCherry^{+} and anti-CaMKII staining in 97.15% ± 2.47% of CaMKII-eGFP^{+}
448 neurons examined. Further, *SCN1A* was expressed in both inhibitory and

449 excitatory neurons of the control and the mutated control lines based on anti-

450 Nav1.1 antibody staining in both GABAergic and glutamatergic neurons (Figure

451 2D).

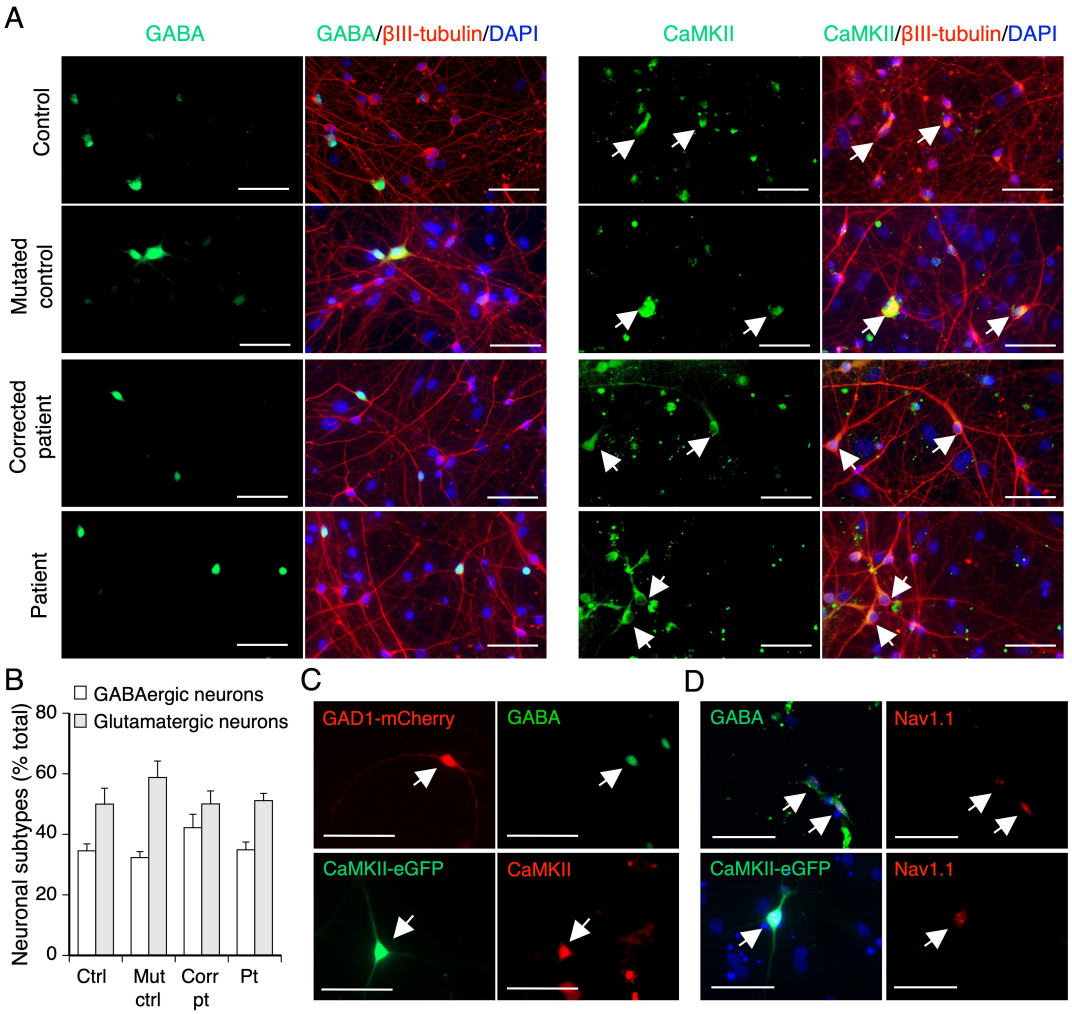

Figure 2. Cultures from two isogenic pairs contain a similar proportion of GABAergic and glutamatergic neurons. (A) Representative micrographs from cultures of two isogenic pairs of iPSC-derived neurons stained with neuronal subtype markers GABA or CaMKII antibodies to identify GABAergic and glutamatergic neurons at D21-24 post plating. (B) The percentage of GABAergic and glutamatergic neurons (white arrows) in neuronal cultures at D21-24 post plating in each line. There was no significant difference between cell lines ($p = 0.1$, one-way ANOVA for GABAergic neurons and $p = 0.6$ Kruskal-Wallis test for glutamatergic neurons). (C) Identification of inhibitory (top) and excitatory (bottom) neurons at D21-24 post plating labeled with plasmids via transient transfection during live recording (white arrows). At least 3 coverslips of 2-3 individual platings were evaluated for each line. (D) Localization of Nav1.1 in GABAergic and glutamatergic neurons of the control line (white arrows). Data represented as mean + s.e.m. Ctrl = control, mut ctrl = mutated control, corr pt = corrected patient, and pt = patient. Scale bar represents 50 μm.

452

453 *3.3. Inhibitory neurons: the K1270T mutation reduces evoked firing and sodium*

454 *current*

455 To determine if the K1270T mutation causes cell type-specific alterations
456 in excitability, evoked action potential recordings were obtained at D21-D24
457 post plating from iPSC-derived inhibitory neurons in cultures from two isogenic
458 pairs: 1a) control (*SCN1A*$^{+/+}$), 1b) mutated control, homozygous (*SCN1A*$^{KT/KT}$);
459 2a) corrected patient (*SCN1A*$^{+/+}$), 2b) patient, heterozygous (*SCN1A*$^{KT/+}$). To
460 account for variability between platings, and within plating, data for all
461 electrophysiological properties represent recordings from multiple cells in at
462 least three independent platings, and these values are presented in each figure
463 or table.

464 Over 90% of inhibitory neurons in each genotype fired action potentials
465 (Figure 3A and 3D). Assessment of firing frequency vs current step curves
466 demonstrated a decrease in mean firing frequency in the homozygous mutated
467 control line compared to the control line (Figure 3B). Both the main effect
468 associated with genotype and an interaction effect for firing frequency were
469 significantly different (genotype: $p = 0.0092$, interaction: $p < 0.0001$, two-way
470 ANOVA with repeated measures; Figure 3B and Table 1). The AP amplitude
471 was also significantly smaller in the homozygous mutated control line compared
472 to the control ($p = 0.0073$, two-tailed unpaired *t* test; Figure 3C).

473 In the heterozygous patient line compared to the corrected patient line,
474 there was no significant decrease in firing frequency associated with the main
475 effect of genotype, but there was a significant interaction effect (genotype: $p =$
476 0.067, interaction: $p = 0.007$, two-way ANOVA with repeated measures; Figure
477 3E and Table 1). This indicates that the firing frequency differed between the

478 two lines depending on the injected currents. Specifically, the heterozygous
479 patient line had decreased firing frequency at small current steps compared to
480 the corrected patient line. However, at current steps of 50 pA and above, the
481 firing frequency of the patient and the corrected patient line were largely
482 overlapping (Figure 3E and Table 1). The AP amplitude in the heterozygous
483 patient line was smaller than that in the corrected patient line, but the difference
484 was not significant (Figure 3F). The reduction in firing frequency and AP firing
485 amplitude in the heterozygous patient line was approximately half that seen in
486 the homozygous mutated line compared to the control line at the low current
487 steps (Figure 3B and 3E and Table 1). These data suggest that the impairment
488 of action potential firing in inhibitory neurons is gene dose-dependent. There
489 were no differences in AP threshold, rheobase, the injected current that first
490 elicited AP firing, and half width within and between isogenic pairs (Table 2).

491 The control and the mutated control had similar input resistance (IR), whole
492 cell capacitance (C_m) and rest membrane potential (RMP; Table 3). Interestingly
493 while the patient line had comparable input resistance to the isogenic corrected
494 line, it had a significantly smaller whole cell capacitance and a more depolarized
495 RMP ($p = 0.024$, and < 0.0001 respectively, Mann-Whitney U test for C_m and
496 unpaired *t* test for RMP; Table 3).

497 To examine whether reduced firing frequency and AP amplitude is
498 associated with alterations in sodium current, isolated sodium currents were
499 recorded in inhibitory neurons at D21-24 post plating. All inhibitory neurons in
500 each genotype expressed sodium currents. Sodium currents were not well
501 space clamped at this age in culture in any of the lines (Figure 3G and 3I),

502 consistent with the localization of some sodium channels at sites electrically
503 distant from the neuronal cell bodies as is typical of neurons that fire multiple
504 APs. This is also consistent with many other studies in which iPSC-derived
505 neurons that are capable of firing a train of APs do not have well clamped
506 sodium currents (Jiao et al., 2013; Kim et al., 2018; Liu et al., 2016, 2013; Sun
507 et al., 2016). However, comparative analysis of sodium current properties
508 between control and patient lines in these studies, as in other published studies,
509 provide insights into the disease mechanism. Therefore, our study focuses on
510 comparing sodium current properties from a family of traces within and between
511 isogenic pairs. While the absolute values may not be reflective of the
512 biophysical properties of sodium currents measured from single channels or in
513 expression systems where there is good voltage control, they allow
514 identification of properties that are or are not associated with the mutation in
515 the native environment.

516 The mean sodium current density versus voltage curves, generated from
517 analysis of inhibitory neurons in each line of an isogenic pair, were compared.
518 The sodium current density in the homozygous mutated control line was
519 reduced compared to the control line. Both the main effect of genotype and an
520 interaction were significant (genotype: $p = 0.050$, interaction: $p = 0.016$, two-
521 way ANOVA with repeated measures; Figure 3G and 3H). In the patient line,
522 heterozygous for the K1270T mutation, there was a similar trend towards a
523 decrease in mean sodium current density at each voltage step above -30 mV
524 compared to the corrected line but the main effect associated with the genotype
525 and the interaction effect were not significantly different (genotype: $p = 0.27$,

526 interaction: $p = 0.33$, two-way ANOVA with repeated measures; Figure 3I and
527 3J).

528 No differences were observed in the voltage-dependence of activation,
529 steady-state inactivation, or recovery from inactivation within the isogenic pairs
530 (the mutated control line compared to the control; the patient compared to the
531 corrected patient line; Figure S2). However, comparison between the isogenic
532 pairs revealed a ~4 mV depolarized shift in voltage dependence of activation in
533 the pair derived from the control compared to the pair derived from the patient
534 (genotype: $p = 0.0065$, interaction: $p < 0.0001$, two-way ANOVA with repeated
535 measures; Table 4 and Figure S2A and S2B). There was also a 3 mV
536 depolarized shift in the voltage dependence of steady-state inactivation in the
537 control vs the patient derived lines (genotype: $p = 0.28$, interaction: $p < 0.0001$,
538 two-way ANOVA with repeated measures; Table 4 and Figure S2C and S2D).
539 Shifts between pairs are likely associated with the genetic background of the
540 GEFS+ patient which would not be found if using unrelated control and patient
541 cell lines. Time constant of recovery from inactivation was similar within
542 isogenic pairs (Table 4 and Figure S2E and S2F).

543 Overall the differences within the isogenic pairs demonstrate that the
544 K1270T mutation causes reduction in evoked firing, action potential amplitude
545 and sodium current density recorded at the cell body in inhibitory neurons. The
546 alterations observed in voltage dependence of activation and steady-state
547 inactivation of sodium currents between isogenic pairs suggest these changes
548 are associated with the genetic background, independent of the mutation.

549

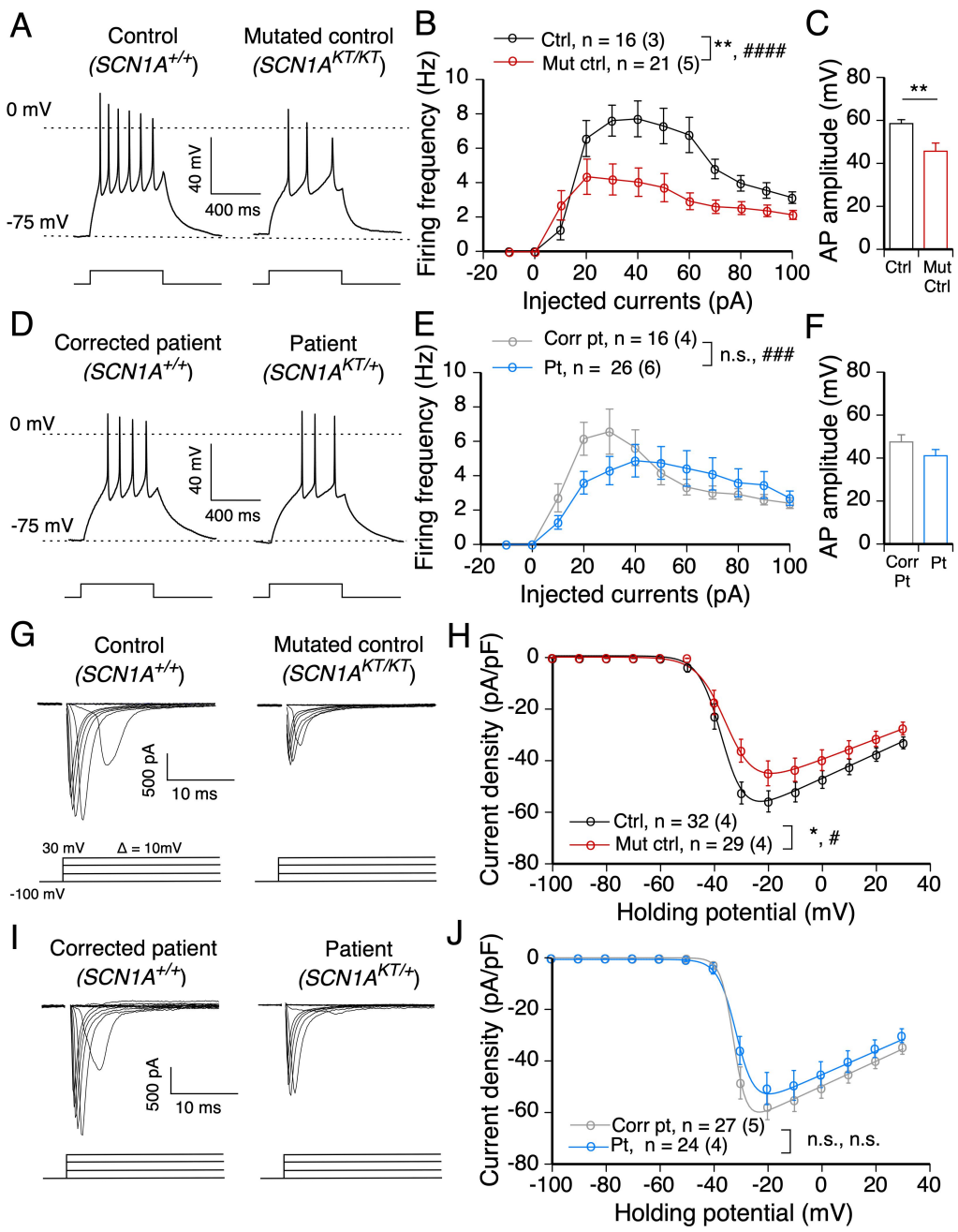

Figure 3. In inhibitory neurons, the K1270T mutation is associated with impaired AP firing and reduced sodium current density. (A) Traces of action potential firing with 30 pA injected in inhibitory neurons of the first isogenic pair of the control (ctrl) and the homozygous mutated control (mut ctrl). (B) The input-output curves of action potentials in inhibitory neurons of the first isogenic pair. (C) AP amplitude of the first AP at rheobase in inhibitory neurons of the first isogenic pair. ** denotes $p < 0.001$, two-tailed unpaired *t*-test. (D-F) Same as A and B, but in inhibitory neurons of the second isogenic pair of the lines from the corrected patient (corr pt) and the heterozygous patient (pt). (G) Traces of voltage-gated sodium currents in inhibitory neurons of the first isogenic pair. The activation protocol started with a prepulse at -100 mV followed by a series of steps ranging from -100 to 30 mV in 10 mV intervals. (H) Current-voltage relationship in inhibitory neurons of the first isogenic pair. Whole cell currents were normalized to capacitance. (I-J) Same as G and H, but in inhibitory neurons of the second isogenic pair. Data presented as mean + s.e.m in C and F, and mean ± s.e.m with total number of neurons evaluated and the number of individual platings in parentheses for each line in B,E,H, and J. * and # represent significant differences in genotypes and interaction within an isogenic pair respectively, two-way ANOVA and *post hoc* Sidak's analysis. One to four symbols denote p values < 0.05, 0.01, 0.001, 0.0001 respectively.

Table 1. Firing frequency of inhibitory neurons

Currents (pA)	Control	Mutated control	Mean change (pair 1)	Corrected patient	Patient	Mean change (pair 2)
-10	0 ± 0	0 ± 0	0	0 ± 0	0 ± 0	0
0	0 ± 0	0 ± 0	0	0 ± 0	0 ± 0	0
10	1.3 ± 0.6	2.7 ± 0.9	1.4	2.7 ± 0.8	1.3 ± 0.4	1.4
20	6.6 ± 1.0	4.4 ± 1.0	2.2	6.1 ± 1.0	3.6 ± 0.7	2.5
30	7.6 ± 0.9	4.2 ± 0.9	3.4	6.6 ± 1.3	4.3 ± 0.8	2.3
40	7.7 ± 1.0	4.0 ± 0.8	3.7	5.6 ± 1.0	4.9 ± 0.9	0.7
50	7.4 ± 1.0	3.7 ± 0.8	3.7	4.2 ± 0.7	4.7 ± 1.0	-0.5
60	6.8 ± 1.0	2.9 ± 0.5	3.9	3.3 ± 0.5	4.4 ± 1.0	-1.1
70	4.8 ± 0.6	2.6 ± 0.4	2.2	3.0 ± 0.4	4.1 ± 0.9	-1.1
80	4.0 ± 0.5	2.5 ± 0.4	1.5	2.9 ± 0.3	3.6 ± 0.8	-0.7
90	3.4 ± 0.5	2.4 ± 0.3	1.0	2.6 ± 0.3	3.5 ± 0.8	-0.9
100	3.1 ± 0.3	2.1 ± 0.3	1.0	2.4 ± 0.3	2.7 ± 0.4	-0.3

a. Data reported as mean ± s.e.m.
b. Two-way ANOVA and *post hoc* Sidak's analysis

Table 2. Measurements of excitability in two isogenic pairs

Cell type	Genotype	Threshold (mV)	Rheobase (pA)	AP half-width (ms)
Inhibitory	Ctrl	-36.2 ± 1.0 n = 13 (3)	18.8 ± 1.7 n = 13 (3)	3.6 ± 0.2 n = 16 (3)
	Mut ctrl	-34.1 ± 1.5 n = 19 (5)	22.5 ± 3.8 n = 16 (5)	4.8 ± 0.6 n = 19 (5)
	Corr pt	-34.8 ± 0.8 n = 16 (4)	15.3 ± 1.7 n = 15 (4)	4.6 ± 0.7 n = 16 (4)
	Pt	-35.4 ± 0.8 n = 25 (6)	23.9 ± 3.3 n = 26 (6)	6.1 ± 0.8 n = 25 (6)
Excitatory	Ctrl	-37.5 ± 1.4 n = 9 (3)	23.3 ± 2.4 n = 9 (3)	3.9 ± 0.4 n = 15 (3)
	Mut ctrl	-36.3 ± 0.8 n = 17 (5)	21.3 ± 1.9 n = 15 (5)	3.9 ± 0.2 n = 29 (5)
	Corr pt	-35.9 ± 1.1 n = 16 (5)	17.5 ± 1.9 n = 16 (5)	4.0 ± 0.5 n = 16 (5)
	Pt	-35.7 ± 0.6 n = 31 (8)	18.7 ± 2.4 n = 32 (8)	4.2 ± 0.2 n = 33 (8)

a. Data reported as mean ± s.e.m with total number of neurons (number of individual platings) underneath.
b. Ctrl = control, mut ctrl = mutated control, corr pt = corrected patient, and pt = patient.
c. Unpaired *t* test for AP threshold, and rheobase in excitatory neurons of the control-derived pair; Mann-Whitney U test for rheobase in inhibitory neurons and excitatory neurons of the patient-derived pair, and AP half-width.

564

Table 3. Comparison of passive membrane properties in two isogenic pairs

565

Cell type	Genotype	IR (GΩ)	C_m (pF)	RMP (mV)
Inhibitory	Ctrl	1.6 ± 0.1 n = 16 (3)	27.3 ± 2.8 n = 15 (3)	-48.0 ± 2.7 n = 13 (3)
	Mut ctrl	1.6 ± 0.1 n = 21 (5)	27.8 ± 2.8 n = 22 (5)	-49.3 ± 2.7 n = 18 (5)
	Corr pt	1.6 ± 0.2 n = 22 (4)	32.1 ± 2.4* n = 22 (4)	-62.8 ± 1.3**** n = 17 (2)
	Pt	1.6 ± 0.1 n = 26 (6)	24.9 ± 2.3 n = 26 (6)	-50.8 ± 2.3 n = 13 (2)
Excitatory	Ctrl	1.0 ± 0.1 n = 16 (3)	30.5 ± 2.5 n = 15 (3)	-52.0 ± 3.2 n = 9 (3)
	Mut ctrl	1.3 ± 0.09* n = 30 (5)	32.6 ± 2.9 n = 28 (5)	-49.9 ± 2.3 n = 17 (5)
	Corr pt	1.3 ± 0.09 n = 24 (5)	31.3 ± 1.4 n = 24 (5)	-56.1 ± 2.0 n = 14 (2)
	Pt	1.5 ± 0.09 n = 48 (8)	36.7 ± 1.8 n = 48 (8)	-54.1 ± 2.4 n = 12 (2)

a. Data reported as mean ± s.e.m with total number of neurons and number of individual platings in parentheses.

573 b. Ctrl = control, mut ctrl = mutated control, corr pt = corrected patient, and pt = patient.

574 c. Statistically significant differences within isogenic pair: * $p < 0.05$ and **** $p < 0.0001$, two-tailed Mann-Whitney U test for IR and C_m and unpaired *t*-test for RMP.

575

Table 4. Comparison of Voltage dependence of Nav in isogenic pairs

Cell type	Line	Activation		Inactivation		Recovery
		$V_{1/2}$ (mV)	k (mV)	$V_{1/2}$ (mV)	k (mV)	τ (ms)
Inhibitory	Ctrl, n = 32 (4)	-38.2 ± 1.4	1.7 ± 0.3	-44.0 ± 1.0	5.5 ± 0.2	3.0 ± 0.2
	Mut ctrl, n = 29 (4)	-35.1 ± 1.4	2.1 ± 0.3	-43.3 ± 0.6	6.3 ± 0.3	3.2 ± 0.2
	Corr pt, n = 27 (5)	-32.0 ± 0.9	2.2 ± 0.3	-41.0 ± 0.4	6.3 ± 0.3	2.8 ± 0.1
	Pt, n =24 (4)	-31.3 ± 1.3	2.5 ± 0.4	-41.0 ± 0.8	6.1 ± 0.3	2.9 ± 0.2
Excitatory	Ctrl, n = 36 (4)	-35.4 ± 1.1	1.7 ± 0.2	-43.2 ± 0.5	5.7 ± 0.1	3.0 ± 0.1
	Mut ctrl, n = 27 (4)	-35.3 ± 1.3	2.2 ± 0.3	-44.0 ± 0.9	5.8 ± 0.2	3.4 ± 0.2
	Corr pt, n = 26 (5)	-31.5 ± 1.0*	2.3 ± 0.3	-42.5 ± 0.7*	7.2 ± 0.5**	2.9 ± 0.1
	Pt, n = 26 (4)	-34.7 ± 1.0	2.0 ± 0.3	-40.5 ± 0.4	5.4 ± 0.2	3.1 ± 0.1

a. Data reported as mean ± s.e.m with total number of neurons and number of individual platings in parentheses for each line.

b. Ctrl = control, mut ctrl = mutated control, corr pt = corrected patient, and pt = patient.

c. Statistically significant differences within isogenic pairs: * $p < 0.05$ and *** $p < 0.001$, two-tailed unpaired *t*-test for activation and inactivation $V_{1/2}$, and Mann-Whitney U test for inactivation k.

576

577 *3.4 Excitatory neurons: the K1270T SCN1A mutation reduces sodium current*

578 *density but does not reduce firing.*

579 Previous studies in iPSC and mouse models have suggested that *SCN1A*

580 mutations reduce evoked firing and sodium currents specifically in inhibitory
581 neurons (Hedrich et al., 2014; Martin et al., 2010; Sun et al., 2016; Yu et al.,
582 2006). However, some studies in other *SCN1A* mutations showed excitability
583 and sodium currents of both excitatory and inhibitory neurons are affected by
584 *SCN1A* mutations (Jiao et al., 2013; Liu et al., 2013; Mistry et al., 2014).
585 Antibody staining demonstrated that both excitatory and inhibitory iPSC-derived
586 neurons in our cultures express Nav1.1 channels. Therefore, it was important
587 to evaluate evoked firing and sodium currents in iPSC-derived excitatory
588 neurons in the same two isogenic pairs examined in the previous section at
589 D21-24 post plating.

590 Over 93% of excitatory neurons in each genotype fired action potentials
591 with injection of depolarizing currents (Figure 4A and 4D). There was no
592 significant main effect difference or interaction effect in the firing frequency
593 versus injected current curves in the homozygous mutated control compared to
594 the control (genotype: $p = 0.91$, interaction: $p = 0.57$, two-way ANOVA with
595 repeated measures; Figure 4B). However, in the heterozygous patient line the
596 firing frequency was significantly increased compared to the corrected patient
597 line at current injections over 30 pA (genotype: $p = 0.041$, interaction: $p =$
598 0.0042, two-way ANOVA with repeated measures; Figure 4E). Since the
599 increased firing frequency in excitatory neurons is only in the patient-derived
600 line and not in the isogenic corrected line or in the control-derived pair (control
601 and mutated control lines), this suggests the phenotype is associated with an
602 interaction between the mutation and the patient genetic background. There
603 was no significant difference in the AP amplitude, threshold, rheobase and AP

604 half-width within or between the isogenic pairs (Figure 4C, 4F and Table 2).

605 The input resistance in the mutated control was slightly higher than that of
606 the control ($p = 0.025$, two-tailed Mann-Whitney U test; Table 3). However, there
607 was no difference in the input resistance between the patient vs the corrected
608 patient line (Table 3). The whole cell capacitance and RMP were similar within
609 the isogenic pairs (Table 3).

610 Based on the lack of decrease in firing in excitatory neurons, and the
611 increase in firing in the patient line, it seemed likely there would be no decrease
612 in sodium current density in the mutated control and possibly an increase in the
613 patient line. To evaluate this, isolated sodium currents were recorded at D21-
614 24 post plating and like inhibitory neurons, all excitatory cells expressed sodium
615 currents that were not well clamped (Figure 4G and 4I). Unexpectedly the
616 current density vs voltage curve demonstrated a significant reduction in sodium
617 current density recorded in the cell body in the homozygous mutated control
618 line compared to the control line (genotype: $p = 0.0025$, interaction: $p < 0.0001$,
619 two-way ANOVA with repeated measures; Figure 4H). The sodium current
620 density in the heterozygous patient line was also smaller compared to the
621 corrected patient line. While the main effect of genotype was not significant,
622 there was a significant interaction effect indicating that sodium current density
623 differed between the two lines depending on the voltage steps (genotype:
624 $p=0.056$, interaction: $p < 0.0001$, genotype, two-way ANOVA with repeated
625 measures; Figure 4J). The reduction of sodium current density in the
626 heterozygous patient line at the higher voltage steps was approximately half
627 the magnitude seen in the homozygous mutated control line (Figure 4H and

628 4J). This is consistent with a gene dose-dependent effect of the mutation.

629 Since there was no concomitant reduction in firing frequency in the
630 excitatory neurons in the homozygous mutant line, this suggests that the
631 properties of other channels, for example potassium channels, in excitatory
632 neurons are more influential in determining the firing phenotype. However, this
633 does not address how a decrease in sodium current in the patient line is
634 consistent with a small but significant increase in excitatory neuron firing
635 frequency. Comparison of other sodium current properties revealed two
636 additional changes in the heterozygous patient line that were not seen in any
637 of the other three lines. There was a hyperpolarized shift in the voltage-
638 dependence of activation and a depolarized shift in steady-state inactivation in
639 the heterozygous patient compared to the corrected patient line ($p = 0.028$ and
640 0.015 respectively, two-tailed unpaired *t* test; Table 4 and Figure S3B and S3D).
641 These alterations are both likely to lead to increased channel opening
642 probability over a larger voltage range that would result in an increased evoked
643 firing rate only in this line (Figure 3F). The differences in activation and steady-
644 state inactivation in only one of the four lines indicate that it is due to an
645 interaction between the K1270T mutation and the patient genetic background.

646 Taken together, similar to the inhibitory neurons, the K1270T mutation
647 causes reduced sodium current density in excitatory neurons. However, the
648 decreased sodium current density caused by the mutation in excitatory neurons
649 is not sufficient to reduce the evoked firing or AP waveforms in the mutated
650 control line. Further, interactions between the mutation and the patient
651 background appear to alter other properties of the sodium channel that increase

652 firing in excitatory neurons of the patient line which may contribute to increased

653 network activity.

654

655

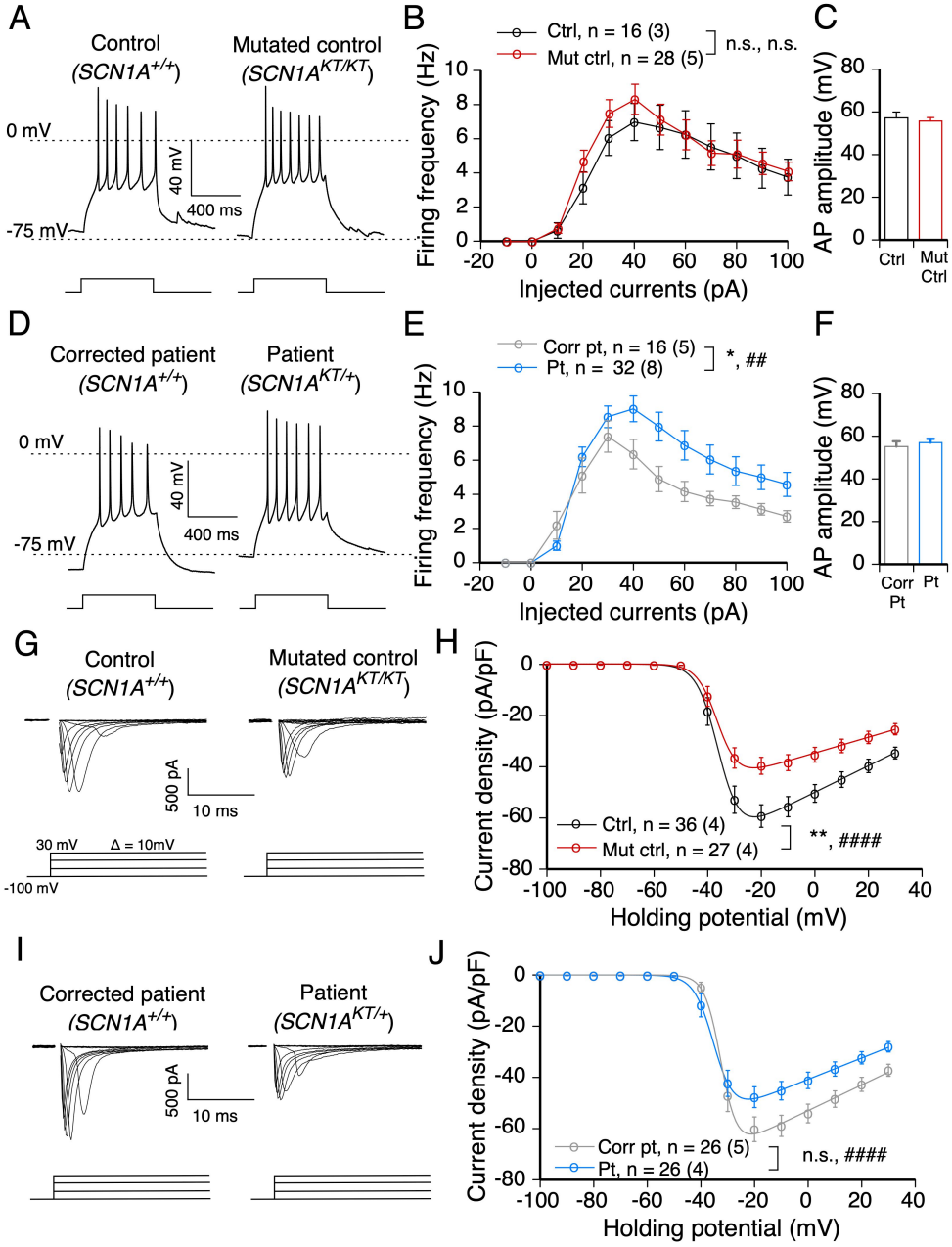

Figure 4. In excitatory neurons, the K1270T mutation affects AP firing and decreases sodium current density. (A) Traces of action potential firing with 30 pA injected in excitatory neurons of the first isogenic pair of the control (ctrl) and the homozygous mutated control (mut ctrl). (B) The input-output curves of action potentials in excitatory neurons of the first isogenic pair. (C) AP amplitude of the first AP at rheobase in excitatory neurons of the first isogenic pair. (D-F) Same as A and B, but in excitatory neurons of the second isogenic pair of the lines of corrected patient (corr pt) and the heterozygous patient (pt). (G) Traces of voltage-gated sodium currents in excitatory neurons of the first isogenic pair. The activation protocol started with a prepulse at -100 mV followed by a series of steps ranging from -100 to 30 mV with a 10 mV interval. (H) Current-voltage relationship in excitatory neurons of the first isogenic pair. Whole cell currents were normalized to capacitance. (I-J) Same as G and H, but in excitatory neurons of the second isogenic pair. Data presented as mean + s.e.m in C and F, and mean ± s.e.m with total number of neurons evaluated and the number of individual platings in parentheses for each line in B,E,H, and J. * and # represent significant differences in genotypes and interaction within an isogenic pair respectively, two-way ANOVA and *post hoc* Sidak's analysis. One to four symbols denote p values < 0.05, 0.01, 0.001, 0.0001 respectively.

657 *3.5. The K1270T mutation results in a hyperexcitable network.*

658 A previous study from our laboratory found that the large majority of
659 neurons in iPSC-derived cultures receive spontaneous glutamatergic and
660 GABAergic synaptic input at D21-24 post plating (Xie et al., 2018). To determine
661 if the K1270T mutation, that specifically reduces firing of inhibitory neurons or
662 increases firing of excitatory neurons in the patient line, causes an increase in
663 excitability of the neuronal network, spontaneous excitatory and inhibitory post-
664 synaptic currents (sEPSCs and sIPSCs) were recorded from excitatory neurons
665 in each genotype.

666 All neurons that received both sEPSCs and sIPSCs were included for
667 analysis. Recordings were obtained at two different holding potentials, -2 mV
668 and -49 mV in each neuron corresponding to the reversal potential for EPSCs
669 and IPSCs, respectively (Figure 5A and 5D). To determine whether there was
670 any change in the balance of excitation vs inhibition, an index, (E-I)/(E+I) was
671 used, where E and I represented amplitude or charge transfer of sEPSC and
672 sIPSC respectively in excitatory neurons. This symmetric index ensures that E
673 and I have the same scale, in contrast to an E/I ratio where the range is
674 asymmetrical. An increase in the (E-I)/(E+I) index indicates an increase in
675 excitatory drive or a decrease in inhibitory drive, and vice versa.

676 The (E-I)/(E+I) index based both on synaptic current amplitude and charge
677 transfer, was significantly larger in the homozygous mutated control line
678 compared to the control and these differences were significant ($p = 0.0002$ and
679 0.046 respectively, two-tailed Mann-Whitney U test; Figure 5B and 5C). There
680 was a similar trend of larger (E-I)/(E+I) index in the heterozygous patient line

compared to the corrected patient line but these differences were not significant (Figure 5E and 5F). This indicates the mutation results in increased excitability in the neural networks formed in these cultures, consistent with the effects of mutation on sodium currents and evoked firing in inhibitory neurons. It also suggests that the increased firing frequency in the excitatory neurons in the patient line does not significantly affect network activity.

To test whether the increased excitatory drive in the network was also influenced by alterations in synaptic vesicle release, miniature excitatory and inhibitory PSCs (mEPSCs and mIPSCs) were recorded in excitatory neurons in the presence of 1 μM tetrodotoxin to block action potentials. The frequency, amplitude, and charge transfer of mEPSCs were similar between genotypes with the same genetic background (Figure S4A-C). There were also no changes in the mIPSCs (Figure S4D-F). This suggests that the K1270T mutation does not affect the synaptic vesicle release.

Together these data indicate that the K1270T mutation results in an imbalance in excitation and inhibition that leads to hyperactivity in the neural network.

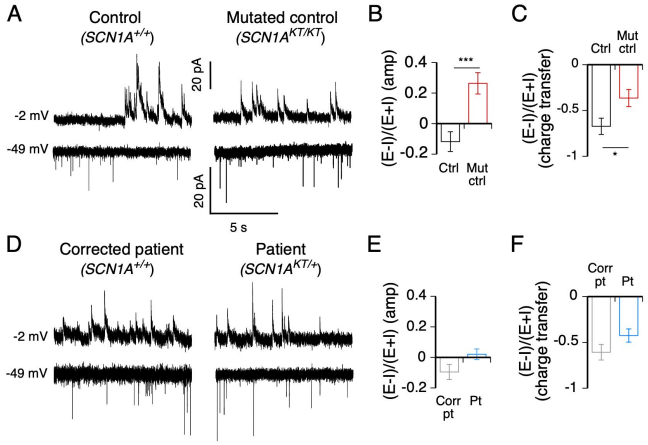

Figure 5. The K1270T mutation gives rise to a hyperactive neural network. (A) Spontaneous excitatory and inhibitory post-synaptic currents received by excitatory neurons in the first isogenic pair of the control (ctrl) and the mutated control (mut ctrl) line. (B) The ratio of spontaneous (E-I)/(E+I) amplitude in excitatory neurons of the first isogenic pair. (C) The ratio of spontaneous (E-I)/(E+I) of charge transfer in excitatory neurons of the first isogenic pair. (D-F) Same as A-C, but in excitatory neurons of the second isogenic pair of the corrected patient (corr pt) and the patient (pt) lines. Data reported as mean ± s.e.m. The total number of neurons and number of platings in parentheses for all four lines are 29 (7), 17 (4), 13 (3), and 18 (3) respectively. *$p < 0.05$ and ***$p < 0.0001$, two-tailed Mann-Whitney U test.

4. Discussion

4.1 Advantages of dual isogenic pair approach

Previous studies have used pairs of isogenic human iPSCs to explore relationship between gene mutations and phenotypes (Ananiev et al., 2011; Bellin et al., 2013; Smith et al., 2018). To our knowledge, ours is the first study to use two pairs of isogenic iPSCs (control sibling vs mutated control, and corrected patient vs patient sibling) to examine the direct relationship, independent of genetic background, between a single ion channel mutation and cellular mechanisms of genetic epilepsy. This approach is an efficient strategy to evaluate the causality of single gene mutations that require analysis at the

715 single cell level to understand cellular mechanisms as is the case for the many
716 different ion channel mutations linked to epilepsy.

717 Mutations that are not only necessary but sufficient to cause the functional
718 change are identified as alterations that occur in both mutant lines, the patient
719 line that carries the endogenous mutation and the mutated control line where
720 K1270T was introduced by CRISPR, and not in the control or corrected patient
721 lines that both lack the mutation but the corrected line has been subjected to
722 CRISPR. In the present study, decreases in firing frequency in inhibitory
723 neurons, and sodium currents in excitatory neurons, in both mutant lines and
724 not in the isogenic controls indicate these phenotypes are due to the K1270T
725 mutation, independent of genetic background. Other changes, AP amplitude
726 and sodium current density in inhibitory neurons and excitatory synaptic drive
727 in excitatory neurons were significant only in the homozygous mutant line
728 compared to its isogenic control. However, changes in the same direction for
729 these properties that were smaller magnitude in the heterozygous line
730 compared to its isogenic control suggest a dose-dependent effect of the
731 K1270T mutation (Table 5). A limitation of this interpretation is that the
732 homozygous and heterozygous mutations are in different genetic backgrounds.
733 To determine how the zygosity of the mutation affects the neuronal activity in
734 the same genetic background, future studies will include generation of a
735 heterozygous mutated control line and a homozygous patient line using
736 CRISPR/Cas9 editing to compare with the existing lines.

737 This comparative strategy also allows for identification of alterations due to
738 the genetic background based on changes that are found in both lines of one

739 isogenic pair but not in the other isogenic pair (Smith et al., 2018), as is seen in
740 the voltage dependence of Nav activation and inactivation in inhibitory neurons
741 of the patient-derived pair only (Table 5). Further, a change in one mutant line
742 that is not seen in the other mutant line or the controls, identifies alterations
743 associated with an interaction between the mutation and the genetic
744 background, as is observed in the voltage dependence of Nav activation and
745 inactivation and increased firing frequency in excitatory neurons of the patient
746 line (Table 5).

747 The GEFS+ patient from whom we collected skin fibroblast had prolonged
748 febrile seizures and generalized afebrile absence seizures that are more severe
749 than other members with the same *SCN1A* mutation in the pedigree (Abou-
750 Khalil et al., 2001). It is likely that genetic background-dependent functional
751 alterations that were observed in the patient line in the current study contribute
752 to the differences in seizure phenotypes between patients in the GEFS+ family.
753 It will be interesting to compare the genetic background of this individual to
754 other GEFS+ family members to identify specific genetic modifiers that
755 exacerbate or ameliorate the cellular defects. For instance, a missense
756 mutation in *SCN9A* that encodes Nav1.7 has been identified in other *SCN1A*-
757 associated epilepsy patients (Singh et al., 2009). To identify genetic modifiers
758 that are altered in the *SCN1A* GEFS+ mutants, single cell RNA sequencing or
759 exome sequencing will be useful for screening candidates in a high-throughput
760 manner (Hawkins et al., 2016; Landis et al., 2017).
761
762
763

764 **Table 5. Origins of effects**

Origin	Mutation independent of background						Genetic background		Interaction between mutation and background		
Cell types	In			Ex			In		Ex		
Properties	AP freq	AP amp	I_{Na^+}	I_{Na^+}	E/I index (amp)	E/I index (Q)	Nav act	Nav inact	AP freq	Nav act	Nav inact
Ctrl	-	-	-	-	-	-	-	-	-	-	-
Mut Ctrl (*SCN1A*$^{KT/KT}$)	↓↓	↓↓	↓↓	↓↓	↑↑	↑↑	-	-	-	-	-
Corr pt	-	-	-	-	-	-	↓	↓	-	-	-
Pt (*SCN1A*$^{KT/+}$)	↓	↓	↓	↓	↑	↑	↓	↓	↑	↓	↑

765 a. Ctrl = control, mut ctrl = mutated control, corr pt = corrected patient, and pt = patient.
766 b. In = inhibitory neurons, ex = excitatory neurons.
767 c. Amp = amplitude of synaptic currents, Q = charge transfer of synaptic currents.
768 d. Nav act = voltage dependence of activation of Nav, Nav inact = voltage dependence of
769 steady-state inactivation of Nav.
770 e. Number of arrows represent fold changes. In properties related to voltage, ↑ and ↓ represent
771 more depolarized and hyperpolarized respectively.
772

773 Transcriptomic analysis in multiple iPSC lines generated from different
774 individuals reveals genetic background variation accounts for differences
775 between lines (Burrows et al., 2016; Rouhani et al., 2014). Therefore, it will be
776 interesting to generate additional cell lines and multiple clones from each line
777 via genome editing to robustly interrogate the interaction between the mutation
778 and genetic background in determining cellular phenotypes.

779

780 *4.2 Alterations in excitability and sodium current density in inhibitory neurons*

781 To examine the cell type-specific effect of the mutation in the
782 electrophysiological properties, inhibitory and excitatory neurons are labeled by
783 transfection of the GAD1-mCherry and CaMKII-eGFP plasmids respectively.
784 Specificity of the labeling was verified by immunostaining with their own

785 markers (Figure 2C). It is unlikely that the majority of the iPSC-derived neurons
786 are of an intermediate phenotype, expressing both GABA and CAMKII, for the
787 following reasons. (1) GABAergic and glutamatergic neurons account for ~35%
788 and ~55% of total neuronal population. If there was a large percentage of
789 neurons that co-express both markers, we would expect to see their additive
790 percentages exceed 100%. (2) The proportion of different neuronal subtypes in
791 cultures is consistent with data from the pharmacology experiment in our
792 previous study in which we found the majority of synaptic connections in neural
793 networks are GABAergic and glutamatergic, and a small population is
794 glycinergic (Xie et al., 2018). (3) Exposure of cultures to a mixture of anti-GABA
795 and anti-CaMKII antibodies resulted in co-labeling with both antibodies in
796 17.8% of GABA+ neurons and 6.7% of CaMKII+ neurons. These were unlikely
797 to be represented in the neuronal population targeted for recording based on
798 their size being less than half of the minimum size targeted for whole cell
799 recordings. Together these data indicate the plasmids label neuronal subtypes
800 with high specificity.

801 Our results demonstrate that in inhibitory neurons, the K1270T *SCN1A*
802 mutation causes decrease in evoked firing frequency and AP amplitude. The
803 reduced excitability and sodium currents in inhibitory neurons is consistent with
804 a number of studies in mouse and iPSC model systems (Martin et al., 2010;
805 Sun et al., 2016; Yu et al., 2006). In particular, previous studies have shown
806 impaired excitability in two subtypes of GABAergic neurons, parvalbumin (PV)-
807 and somatostatin (SST)-expressing interneurons in mouse models of *SCN1A*
808 epilepsy (Favero et al., 2018; Tai et al., 2014). Selective deletion of *Scn1a* in
809 PV and SST interneurons causes hyperactivity in neural networks and seizure

810 behaviors, suggesting the importance of Nav1.1 in regulating inhibitory neuron
811 activity and the E/I balance (Cheah et al., 2012; Dutton et al., 2013; Rubinstein
812 et al., 2015). Our preliminary data reveal that GABAergic neurons in our
813 cultures can be divided into at least two groups staining iPSC-derived neurons
814 with anti-βIII-tubulin and PV or SST antibodies (data not shown). However, we
815 did not observe fast spiking, bursting or adapting firing patterns characteristic
816 of PV and SST interneurons in recorded GAD1-mCherry^{+} neurons. This
817 suggests that functional maturation of interneuron subtypes require a longer
818 time in culture. Future studies will be directed to determine the effect of *SCN1A*
819 mutation in the electrophysiological properties of identified PV and SST
820 interneurons.

821 iPSC-derived inhibitory neurons in the present study had large sodium
822 currents, but they were not well space clamped. This is typical in neurons that
823 are capable of firing multiple APs (Jiao et al., 2013; Kim et al., 2018; Liu et al.,
824 2016, 2013; Sun et al., 2016). While evaluation of sodium currents that are not
825 well space clamped does not resolve absolute biophysical properties,
826 comparisons of sodium current properties within and between isogenic pairs
827 are still informative in identifying alterations caused by the mutation. For
828 example, pair wise comparisons demonstrate that the K1270T mutation causes
829 a decrease in sodium current density in inhibitory neurons. Further studies will
830 be necessary to determine if the reduction in sodium current density recorded
831 at the cell bodies is due to a decrease in total number of sodium channels
832 expressed or a change in localization of channels as channels distant from the
833 cell soma might reduce their contribution to the recorded currents. This could

834 be addressed by immune-electron microscopy to evaluate voltage-gated
835 sodium channel localization in neurons from the different genotypes.
836
837 *4.3 Alterations in excitability and sodium current density in excitatory neurons*
838 Previous studies have reported mutation of *SCN1A* has little effect on
839 sodium currents in excitatory neurons (Martin et al., 2010; Sun et al., 2016; Yu
840 et al., 2006). In contrast we report that the K1270T mutation results in a similar
841 decrease in sodium current density in excitatory and inhibitory neurons. This is
842 consistent with Nav1.1 staining not only in GABAergic neurons but in our
843 CaMKII-eGFP$^+$ neurons. While previous studies suggest that Nav1.1 is strongly
844 expressed in inhibitory neurons (Ogiwara et al., 2007), other studies report that
845 Nav1.1 is present in a subset of excitatory neurons (Dutton et al., 2013;
846 Ogiwara et al., 2013).
847 Interestingly, the decrease in sodium current density does not result in
848 reduced firing in the excitatory neurons as it does in inhibitory neurons. This
849 indicates that the changes in the sodium current density were not sufficient to
850 reduce excitability in this cell type. This could be due to compensation from
851 potassium currents, as a voltage-gated potassium channel Kv8.2 has been
852 shown to function as a genetic modifier increasing the susceptibility of an *Scn2a*
853 mutant mouse to epilepsy (Bergren et al., 2009; Jorge et al., 2011). Altered
854 currents of Kv1 and Kv4 are associated with increased excitability in a subset
855 of pyramidal neurons in a mouse model of fragile X syndrome (Kalmbach et al.,
856 2015). *CACNB4* and *CACNA1A* that encode Cav have also been identified as
857 genetic modifiers that result in a gain of function in families with *SCN1A* Dravet

858 syndrome (Ohmori et al., 2013, 2008).

859 Further, the AP firing frequency is actually increased in the excitatory
860 neurons in the patient line resulting from an interaction between the mutation
861 and the patient genetic background. This is consistent with changes in the
862 voltage-dependence of sodium current activation and inactivation only in the
863 patient excitatory neurons. These changes predict that the channel is open over
864 a wider voltage range and is thus consistent with the increase in AP firing seen
865 in patient excitatory neurons. To explore the biophysical changes in finer detail
866 it would be possible to lower the external sodium concentration to reduce the
867 size of the sodium currents and increase potential for good voltage control
868 (Colatsky, 1980). One could also examine the biophysical properties of single
869 sodium channels in excised or cell attached patches from the cell body
870 (Franciolini, 1986; Stühmer et al., 1987). Both of these would provide additional
871 insight, but they also have the limitation of restricting analysis to a small
872 population of channels in a restricted location (on or near cell body) that may
873 not represent the full population of channels that define the firing properties of
874 the neurons.

875

876 *4.4 Hyperactive neural network*

877 Our previous study demonstrates that iPSC-derived neurons form
878 functionally active neural networks that contain GABAergic and glutamatergic
879 synaptic connections (Xie et al., 2018), allowing us to evaluate the effect the
880 K1270T mutation on the network activity of the neuronal cultures. Our results
881 reveal an increase in excitatory drive relative to inhibitory drive in excitatory

882 neurons.

883 There are no significant differences in the (E-I)/(E+I) index on the basis of
884 sPSC frequency between the two lines within the same isogenic pairs.
885 Therefore, it is likely that alteration in the index based on charge transfer is
886 associate with that on PSC amplitude. However, how a mutation in Nav leads
887 to increased PSC amplitude is still unclear. It is likely that homeostatic
888 regulation in genes that encode post-synaptic receptors is involved. Future
889 studies will include examination of expression of glutamate receptors such as
890 NMDA and AMPA receptors and GABA receptors such as $GABA_A$ receptors etc.

891 Hyperexcitable neural networks are implicated in epileptic disorders (Shao
892 et al., 2019). Therefore, our iPSC-derived neuronal cultures provide insights
893 into the underlying mechanism of how an epilepsy-associated *SCN1A* mutation
894 gives rise to increased probability of seizures in patients. To understand the
895 effect of the mutation on the spontaneous network activity and network
896 synchrony more broadly, our future studies will use multi-electrode arrays that
897 allow for mechanistic study and anti-epileptic drug screening in a high-
898 throughput manner (Tidball and Parent, 2016).

899

900 *4.5 Developmental maturation*

901 Using our neuronal differentiation protocol that includes plating iPSC-
902 derived neural progenitors onto astroglial feeder layers, the large majority of
903 neurons fire multiple action potentials (Schutte et al., 2018; Xie et al., 2018).
904 The derived neurons not only have sodium currents larger than 1 nA in average
905 and fire multiple action potentials at 7-8 Hz comparable to other iPSC studies
906 (Liu et al., 2013; Sun et al., 2016), but they also receive glutamatergic and

907 GABAergic synaptic input within 3 weeks of plating. However, their
908 electrophysiological properties are less mature than neurons expected in an
909 adult brain, based on lower firing frequency, larger input resistance, and
910 depolarized RMP. Single-cell transcriptome analysis reveals development of
911 interneurons at D54 *in vitro* recapitulates those in human fetal cortex at 100 dpc
912 (Close et al., 2017). While we cannot rule out the possibility that the K1270T
913 mutation causes a developmental delay in neuronal development in culture, it
914 seems unlikely to explain our results of reduced firing frequency and action
915 potential AP in inhibitory neurons associated with the mutation because 1) there
916 was no consistent change in RMP or input resistance and 2) the excitatory
917 neurons of the mutated control and the patient lines were able to fire APs in
918 similar or higher frequency compared to their controls. However future studies
919 could evaluate effects of the mutation on further maturation in long-term
920 cultures.
921
922 *4.6 Off-target mutation*
923 Sequences of the top five off-target sites from CRISPR/Cas9 editing,
924 including *SCN7A*, *FLII*, *SCN2A*, *SCN3A* and *SCN9A* were examined. The
925 corrected patient line did not have off-target mutations in the candidate genes
926 (Supplementary Figure 1A). While the mutated control line did not have off-
927 target mutations in the other genes, it harbored one in *SCN7A*. It is very unlikely
928 that this mutation affected the results reported based on the following
929 considerations. First, *SCN7A* encodes the Na_x sodium channel in heart, uterus,
930 skeletal muscle, and peripheral nervous system (Goldin et al., 2000) and RT-

931 PCR analysis demonstrated that it is not expressed in our iPSC-derived
932 neurons of the mutated control line (Supplementary Figure 1B). Secondly, the
933 channel is insensitive to changes in membrane potential and TTX, a voltage-
934 gated sodium channel blocker (Hiyama et al., 2002). Isolated sodium currents
935 in iPSC-derived neurons at D21-24 post plating were completely eliminated in
936 the presence of 1 μM TTX (Supplementary Figure 1C). Third, while it is possible
937 that the off-target mutation in *SCN7A* could trigger homeostatic regulation by
938 up- or down-regulating *SCN1A* expression, this is unlikely as the alterations in
939 sodium currents/evoked firing in the homozygous mutated control line were in
940 the same direction and twice as large as the heterozygous patient line that did
941 not undergo editing process.
942
943 *4.7 Comparison with the previous knock-in fly model*
944 The reduced excitability observed specifically in iPSC-derived inhibitory
945 neurons is consistent with the decreased excitability specifically in inhibitory
946 neurons in the brains of K1270T GEFS+ knock-in *Drosophila* (Sun et al., 2012).
947 Since both flies and patients exhibit heat-induced seizures, this provides
948 additional support to the hypothesis that reduced firing specifically in inhibitory
949 neurons is critical to the disease phenotype in humans. However, the cellular
950 defect associated with reduced excitability is distinct between the models
951 demonstrating two independent mechanisms that result in a similar phenotype.
952 In the iPSC-derived neurons there is a significant decrease in the amplitude of
953 the transient currents that are the dominant form of sodium current in these
954 neurons. In flies the reduced firing is associated with a hyperpolarized shift in

955 the deactivation threshold of the large persistent sodium currents characteristic
956 of inhibitory neurons in the adult fly brain. It is possible that modifying the
957 persistent currents in iPSCs by shifting their voltage dependence could
958 moderate the deficits associated with a reduced transient sodium current.

959 In addition, an increase in excitability was observed in excitatory neurons
960 of the patient line, consistent with the higher firing rate in excitatory neurons in
961 the GEFS+ flies (Schutte et al., 2016). The alterations in fly are seen
962 predominantly at high temperature, so it is possible that elevated temperatures
963 will reveal additional or more severe alterations in sodium currents in iPSC-
964 derived neurons, as the patient sibling from whom the skin fibroblast was
965 collected showed more severe seizure phenotypes of febrile seizures
966 compared to afebrile seizures (Abou-Khalil et al., 2001).

967

968 *4.8 Summary*

969 Overall the CRISPR/Cas9-based disease modeling strategy with iPSC-
970 derived neurons can validate clinically relevant phenotypes and reveal the
971 sufficiency and necessity of *SCN1A* mutations for specific phenotypes in the
972 human genetic background. Furthermore, a library of patient iPSCs with a
973 variety of *SCN1A* mutations built using this approach, in combination with a
974 high-throughput drug screening method such as multi-electrode array (MEA),
975 will facilitate the development of personalized anti-epileptic medicine (Du and
976 Parent, 2015; Odawara et al., 2016; Parent and Anderson, 2015).

977

5. Supplemental information

Supplementary Table 1. Primers for off-target gene sequencing and expression

Gene	Reference	Direction	Sequence
Off-target gene sequencing			
SCN7A	NG_031928.1	Fwd	5' ACAAGCATAGTGAACCAGCCCT 3'
		Rev	5' GATCAGCCCTGCACTTGTGAAC 3'
FLII	NG_023243.1	Fwd	5' GGCTGCAGACAAGAGCAAGAAA 3'
		Rev	5' CACAGCTGTTCTTTCTGCCCAG 3'
SCN9A	NG_012798.1	Fwd	5' CAGCACTGGTGAGAAGGCTAGA 3'
		Rev	5' ACTTGATGTGCCCCTCATCCTC 3'
SCN2A	NG_008143.1	Fwd	5' CCCTTGGTTGACTGAAATGCCC 3'
		Rev	5' TGCGAAATGTGAGTGTGCAAAA 3'
SCN5A	NG_008934.1	Fwd	5' GGAGAATCACTTGAACCCGGGA 3'
		Rev	5' GGCAGGACCCTGTCTCCTATTT 3'
SCN3A	NG_042289.1	Fwd	5' TTCCCTGCCAGCATTTTCACAC 3'
		Rev	5' ACAATTCTCCCTGTGTTTGCTCT 3'
Off-target gene expression			
SCN1A	NM_001165963.2	Fwd (ext)	5' TCCTTCGGGATCCATGGAACTG 3'
		Rev (ext)	5' CGTTTTCCCAGCAGCACGTAAT 3'
		Fwd (int)	5' TGTCTCGGCATTGAGAACATTC 3'
		Rev (int)	5' ATTGGTGGGAGGCCATTGTAT 3'
SCN7A	NM_002976.3	Fwd (ext)	5' AGCTGAGGGAAAACTAGTGCCC 3'
		Rev (ext)	5' GTGGATCAGGACCCCTACAAGG 3'
		Fwd (int)	5' AGAACCTAAGGGCCTTGTTCCC 3'
		Rev (int)	5' ACACAAGATGGAAGCCGCATTG 3'
ACTB	NM_001101.5	Fwd	5' CCACCATGTACCCTGGCATT 3'
		Rev	5' ACTCCTGCTTGCTGATCCAC 3'

a. Off-target gene expression was examined by nested PCR that uses two sets of primers.
b. Fwd, rev, ext and int are abbreviated for forward, reverse, external set and internal set of primers.

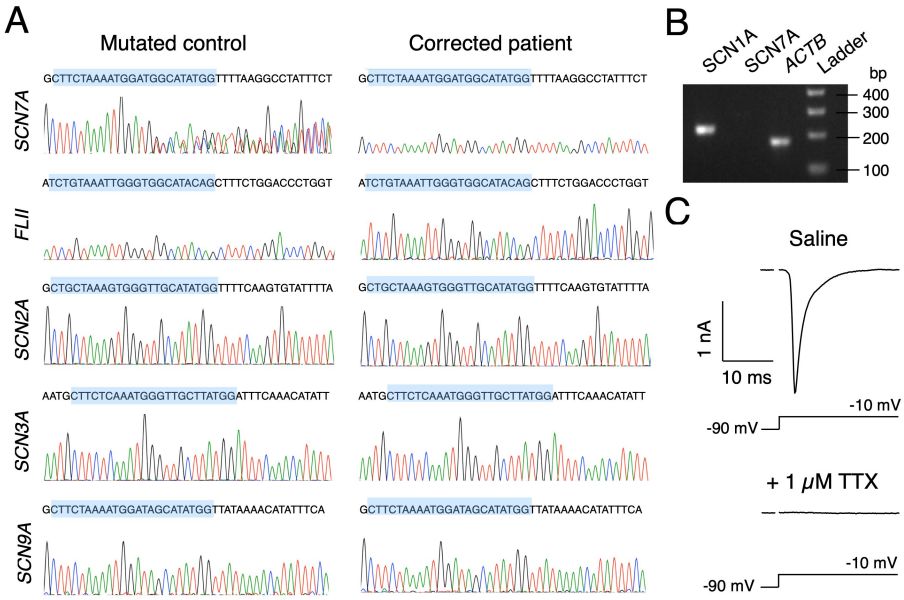

Supplementary Figure 1 related to Figure 1. (A) Sequences of the top five predicted off-target sites in *SCN7A*, *FLII, SCN2A*, *SCN3A* and *SCN9A*. Off-target mutation was identified in the *SCN7A* gene of the mutated control line. Regions highlighted in blue are the sites predicted to be modified by non-specific CRISPR/Cas9 editing. (B) Expression of *SCN1A*, *SCN7A* and the housekeeping gene *ACTB* in the derived neurons of the mutated control line at D21 post plating. Expected band sizes of *SCN1A*, *SCN7A* and *ACTB* are 220, 283 and 177 bp. (C) Isolated sodium current recording in the derived neurons of the control line at D54 post plating. Sodium currents were completely eliminated in the presence of 1 μM TTX.

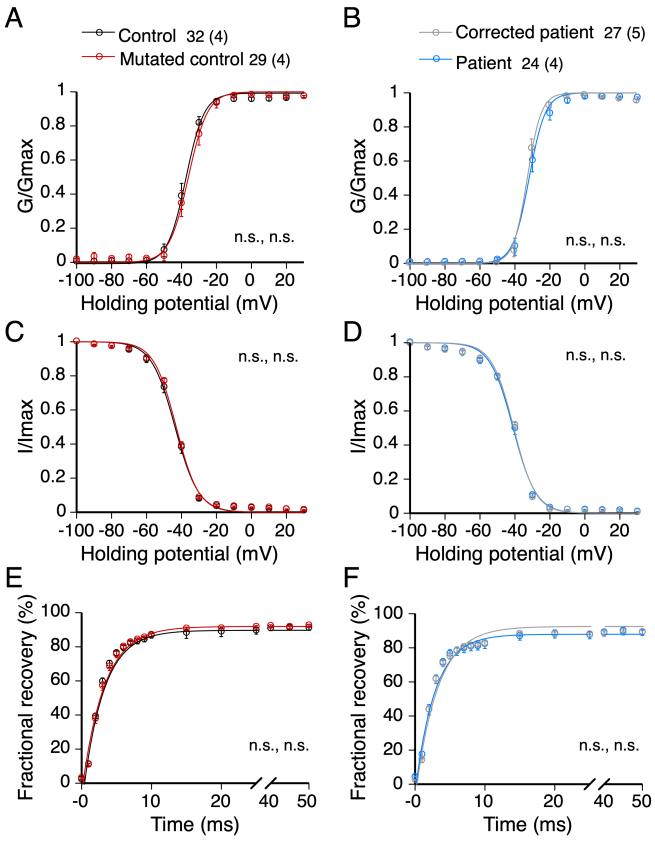

Supplementary Figure 2 related to Figure 3. Properties of Nav in inhibitory neurons. (A-B) Conductance vs voltage curves of activation in inhibitory neurons of the control vs the mutated control lines, and the corrected patient vs the patient lines respectively. (C-D) Current vs voltage curves of steady-state inactivation in inhibitory neurons of isogenic pairs. (E-F) Recovery of inactivation in both isogenic pairs. Data presented as mean ± s.e.m with total number of neurons and number of individual platings in parentheses evaluated in each line. Two-way ANOVA and *post hoc* Sidak's analysis.

1002

1003

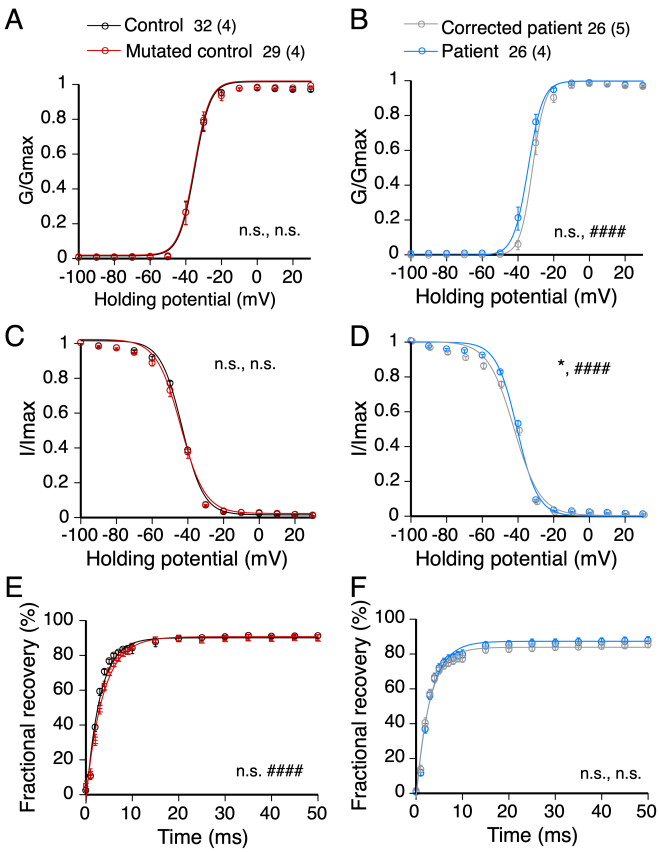

Supplementary Figure 3 related to Figure 4. Properties of Nav in excitatory neurons. (A-B) Conductance vs voltage curves of activation in excitatory neurons of the control vs the mutated control lines, and the corrected patient vs the patient lines respectively. (C-D) Current vs voltage curves of steady-state inactivation in excitatory neurons of isogenic pairs. (E-F) Recovery of inactivation in both isogenic pairs. Data presented as mean ± s.e.m with total number of neurons and number of individual platings in parentheses. * and # represent significant differences in genotypes and interaction within an isogenic pair respectively, two-way ANOVA and *post hoc* Sidak's analysis. One and four symbols denote p values < 0.05, and 0.0001 respectively.

1004

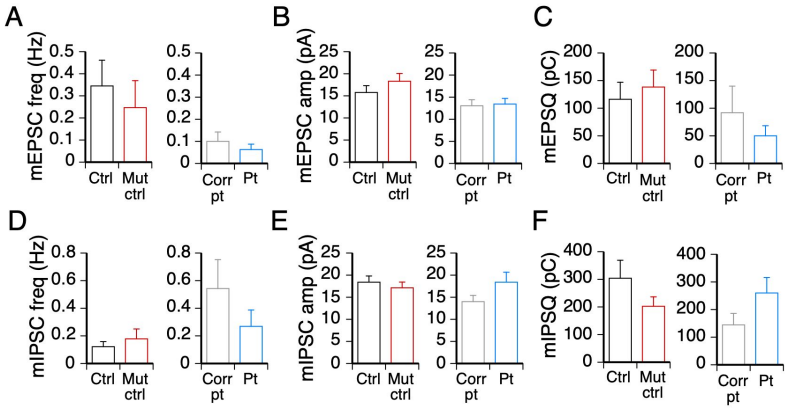

Supplementary Figure 4 related to Figure 5. Miniature EPSCs IPSCs received by excitatory neurons were unaltered by the K1270T mutation. (A-C) The frequency, amplitude and charge transfer of mEPSCs in the control (ctrl) vs the mutated control (mut ctrl), and the corrected patient (corr pt) vs the patient (pt) lines. (D-F) Same as A-C, but for mIPSCs. Data reported as mean + s.e.m. The total number of neurons and number of individual platings in parentheses for all four lines are ctrl: 9 (5), mut ctrl: 7 (3), corr pt:10 (4), and pt:10 (3).

1005

1006 **6. Acknowledgement**

1007 This work was supported by the National Institutes of Health grants R01
1008 NS083009 (D.K.O.), R01 GHD059967 grant (P.H.S.), and R01 NS078289
1009 (K.C.E.) and a California Institute for Regenerative Medicine Bridges to Stem
1010 Cell Research grant CIRM-EDUC2-08383 (C.M.R.). We would also like to thank
1011 Alexander E. Stover for generating the iPSCs, Priscilla Figueroa, Noor Osman
1012 and Daniel R. Benavides for help on astroglial cultures, Sara E. Konopelski for
1013 help on screening of clones, Karla Soto Sauza for help on immunostaining and
1014 cell counting and Longwen Huang for input on the manuscript.

1015

1016 **7. Author contributions**

1017 The laboratory of K.C.E. provided skin fibroblasts from the unaffected sibling

1018 and the patient sibling from the GEFS+ family. The laboratory of P.H.S.
1019 reprogrammed the fibroblasts into iPSCs. O.S.S. and M.A.S. designed the
1020 CRISPR/Cas9, and O.S.S., Y.X., N.N.N. and C.M.R. performed screening of
1021 positive clones. C.M.R., N.N.N., O.S.S. and Y.X. prepared astroglial cultures.
1022 Y.X., N.N.N. and C.M.R differentiated iPSCs into neurons. Y.X. and N.N.N.
1023 performed electrophysiological recording. Y.X., N.N.N. and C.M.R analyzed the
1024 electrophysiology data. Y.X. and N.N.N. performed immunostaining, imaging
1025 and cell counting. Y.X. wrote the manuscript, N.N.N., O.S.S., K.C.E, P.H.S.,
1026 M.A.S. and D.K.O. edited the manuscript.
1027

1028 **References**

1029 Abou-Khalil, B., Ge, Q., Desai, R., Ryther, R., Bazyk, A., Bailey, R., Haines,
1030 J.L., Sutcliffe, J.S., George, A.L.J., 2001. Partial and generalized epilepsy
1031 with febrile seizures plus and a novel SCN1A mutation. Neurology 57,
1032 2265–2272.

1033 Ananiev, G., Williams, E.C., Li, H., Chang, Q., 2011. Isogenic pairs of wild type
1034 and mutant induced pluripotent stem cell (iPSC) lines from Rett syndrome
1035 patients as in vitro disease model. PLoS One 6, e25255–e25255.
1036 https://doi.org/10.1371/journal.pone.0025255

1037 Bassett, A.R., 2017. Editing the genome of hiPSC with CRISPR/Cas9: disease
1038 models. Mamm. Genome 28, 348–364. https://doi.org/10.1007/s00335-
1039 017-9684-9

1040 Baulac, S., Huberfeld, G., Gourfinkel-An, I., Mitropoulou, G., Beranger, A.,
1041 Prud'homme, J.F., Baulac, M., Brice, A., Bruzzone, R., LeGuern, E., 2001.

1042 First genetic evidence of GABA(A) receptor dysfunction in epilepsy: a
1043 mutation in the gamma2-subunit gene. Nat. Genet. 28, 46–48.
1044 https://doi.org/10.1038/88254
1045 Bellin, M., Casini, S., Davis, R.P., D'Aniello, C., Haas, J., Ward-van Oostwaard,
1046 D., Tertoolen, L.G.J., Jung, C.B., Elliott, D.A., Welling, A., Laugwitz, K.-L.,
1047 Moretti, A., Mummery, C.L., 2013. Isogenic human pluripotent stem cell
1048 pairs reveal the role of a KCNH2 mutation in long-QT syndrome. EMBO J.
1049 32, 3161–3175. https://doi.org/10.1038/emboj.2013.240
1050 Bergren, S.K., Rutter, E.D., Kearney, J.A., 2009. Fine mapping of an epilepsy
1051 modifier gene on mouse Chromosome 19. Mamm. Genome 20, 359–366.
1052 https://doi.org/10.1007/s00335-009-9193-6
1053 Burrows, C.K., Banovich, N.E., Pavlovic, B.J., Patterson, K., Gallego Romero,
1054 I., Pritchard, J.K., Gilad, Y., 2016. Genetic Variation, Not Cell Type of
1055 Origin, Underlies the Majority of Identifiable Regulatory Differences in
1056 iPSCs. PLOS Genet. 12, e1005793.
1057 Cheah, C.S., Yu, F.H., Westenbroek, R.E., Kalume, F.K., Oakley, J.C., Potter,
1058 G.B., Rubenstein, J.L., Catterall, W.A., 2012. Specific deletion of NaV1.1
1059 sodium channels in inhibitory interneurons causes seizures and premature
1060 death in a mouse model of Dravet syndrome. Proc. Natl. Acad. Sci. U. S.
1061 A. 109, 14646–14651. https://doi.org/10.1073/pnas.1211591109
1062 Chen, W., Liu, J., Zhang, L., Xu, H., Guo, X., Deng, S., Liu, L., Yu, D., Chen, Y.,
1063 Li, Z., 2014. Generation of the SCN1A epilepsy mutation in hiPS cells using
1064 the TALEN technique. Sci. Rep. 4, 5404.
1065 Close, J.L., Yao, Z., Levi, B.P., Miller, J.A., Bakken, T.E., Menon, V., Ting, J.T.,

1066 Wall, A., Krostag, A.-R., Thomsen, E.R., Nelson, A.M., Mich, J.K., Hodge,
1067 R.D., Shehata, S.I., Glass, I.A., Bort, S., Shapovalova, N. V, Ngo, N.K.,
1068 Grimley, J.S., Phillips, J.W., Thompson, C.L., Ramanathan, S., Lein, E.,
1069 2017. Single-Cell Profiling of an In Vitro Model of Human Interneuron
1070 Development Reveals Temporal Dynamics of Cell Type Production and
1071 Maturation. Neuron 93, 1035-1048.e5.
1072 https://doi.org/10.1016/j.neuron.2017.02.014
1073 Colatsky, T.J., 1980. Voltage clamp measurements of sodium channel
1074 properties in rabbit cardiac Purkinje fibres. J. Physiol. 305, 215–234.
1075 Dibbens, L.M., Feng, H.-J., Richards, M.C., Harkin, L.A., Hodgson, B.L., Scott,
1076 D., Jenkins, M., Petrou, S., Sutherland, G.R., Scheffer, I.E., Berkovic, S.F.,
1077 Macdonald, R.L., Mulley, J.C., 2004. GABRD encoding a protein for extra-
1078 or peri-synaptic GABAA receptors is a susceptibility locus for generalized
1079 epilepsies. Hum. Mol. Genet. 13, 1315–1319.
1080 https://doi.org/10.1093/hmg/ddh146
1081 Du, X., Parent, J.M., 2015. Using Patient-Derived Induced Pluripotent Stem
1082 Cells to Model and Treat Epilepsies. Curr. Neurol. Neurosci. Rep.
1083 https://doi.org/10.1007/s11910-015-0588-3
1084 Dutton, S.B., Makinson, C.D., Papale, L.A., Shankar, A., Balakrishnan, B.,
1085 Nakazawa, K., Escayg, A., 2013. Preferential inactivation of Scn1a in
1086 parvalbumin interneurons increases seizure susceptibility. Neurobiol.
1087 Dis. 49, 211–220. https://doi.org/10.1016/j.nbd.2012.08.012
1088 Escayg, A., Heils, A., MacDonald, B.T., Haug, K., Sander, T., Meisler, M.H.,
1089 2001. A novel SCN1A mutation associated with generalized epilepsy with

1090 febrile seizures plus--and prevalence of variants in patients with epilepsy.
1091 Am. J. Hum. Genet. 68, 866–873. https://doi.org/10.1086/319524
1092 Escayg, A., MacDonald, B.T., Meisler, M.H., Baulac, S., Huberfeld, G., An-
1093 Gourfinkel, I., Brice, A., LeGuern, E., Moulard, B., Chaigne, D., Buresi, C.,
1094 Malafosse, A., 2000. Mutations of SCN1A, encoding a neuronal sodium
1095 channel, in two families with GEFS+2. Nat. Genet. 24, 343–345.
1096 https://doi.org/10.1038/74159
1097 Favero, M., Sotuyo, N.P., Lopez, E., Kearney, J.A., Goldberg, E.M., 2018. A
1098 Transient Developmental Window of Fast-Spiking Interneuron Dysfunction
1099 in a Mouse Model of Dravet Syndrome. J. Neurosci. 38, 7912–7927.
1100 https://doi.org/10.1523/JNEUROSCI.0193-18.2018
1101 Franciolini, F., 1986. Patch clamp technique and biophysical study of
1102 membrane channels. Experientia 42, 589–594.
1103 https://doi.org/10.1007/BF01955551
1104 Gautron, S., Dos Santos, G., Pinto-Henrique, D., Koulakoff, A., Gros, F.,
1105 Berwald-Netter, Y., 1992. The glial voltage-gated sodium channel: cell- and
1106 tissue-specific mRNA expression. Proc. Natl. Acad. Sci. U. S. A. 89, 7272–
1107 7276. https://doi.org/10.1073/pnas.89.15.7272
1108 Goldberg-Stern, H., Aharoni, S., Afawi, Z., Bennett, O., Appenzeller, S.,
1109 Pendziwiat, M., Kuhlenbaumer, G., Basel-Vanagaite, L., Shuper, A.,
1110 Korczyn, A.D., Helbig, I., 2014. Broad phenotypic heterogeneity due to a
1111 novel SCN1A mutation in a family with genetic epilepsy with febrile
1112 seizures plus. J. Child Neurol. 29, 221–226.
1113 https://doi.org/10.1177/0883073813509016

1114 Goldin, A.L., Barchi, R.L., Caldwell, J.H., Hofmann, F., Howe, J.R., Hunter, J.C.,
1115 Kallen, R.G., Mandel, G., Meisler, M.H., Netter, Y.B., Noda, M., Tamkun,
1116 M.M., Waxman, S.G., Wood, J.N., Catterall, W.A., 2000. Nomenclature of
1117 Voltage-Gated Sodium Channels. Neuron 28, 365–368.
1118 https://doi.org/10.1016/S0896-6273(00)00116-1
1119 Harkin, L.A., Bowser, D.N., Dibbens, L.M., Singh, R., Phillips, F., Wallace, R.H.,
1120 Richards, M.C., Williams, D.A., Mulley, J.C., Berkovic, S.F., Scheffer, I.E.,
1121 Petrou, S., 2002. Truncation of the GABA(A)-receptor gamma2 subunit in
1122 a family with generalized epilepsy with febrile seizures plus. Am. J. Hum.
1123 Genet. 70, 530–536. https://doi.org/10.1086/338710
1124 Hawkins, N.A., Zachwieja, N.J., Miller, A.R., Anderson, L.L., Kearney, J.A.,
1125 2016. Fine Mapping of a Dravet Syndrome Modifier Locus on Mouse
1126 Chromosome 5 and Candidate Gene Analysis by RNA-Seq. PLOS Genet.
1127 12, e1006398.
1128 Hedrich, U.B.S., Liautard, C., Kirschenbaum, D., Pofahl, M., Lavigne, J., Liu,
1129 Y., Theiss, S., Slotta, J., Escayg, A., Dihne, M., Beck, H., Mantegazza, M.,
1130 Lerche, H., 2014. Impaired action potential initiation in GABAergic
1131 interneurons causes hyperexcitable networks in an epileptic mouse model
1132 carrying a human Na(V)1.1 mutation. J. Neurosci. 34, 14874–14889.
1133 https://doi.org/10.1523/JNEUROSCI.0721-14.2014
1134 Higurashi, N., Uchida, T., Lossin, C., Misumi, Y., Okada, Y., Akamatsu, W.,
1135 Imaizumi, Y., Zhang, B., Nabeshima, K., Mori, M.X., Katsurabayashi, S.,
1136 Shirasaka, Y., Okano, H., Hirose, S., 2013. A human Dravet syndrome
1137 model from patient induced pluripotent stem cells. Mol. Brain 6, 19.

https://doi.org/10.1186/1756-6606-6-19

Hiyama, T.Y., Watanabe, E., Ono, K., Inenaga, K., Tamkun, M.M., Yoshida, S., Noda, M., 2002. Nax channel involved in CNS sodium-level sensing. Nat. Neurosci. 5, 511–512. https://doi.org/10.1038/nn0602-856

Jiao, J., Yang, Y., Shi, Y., Chen, J., Gao, R., Fan, Y., Yao, H., Liao, W., Sun, X.-F., Gao, S., 2013. Modeling Dravet syndrome using induced pluripotent stem cells (iPSCs) and directly converted neurons. Hum. Mol. Genet. 22, 4241–4252. https://doi.org/10.1093/hmg/ddt275

Jorge, B.S., Campbell, C.M., Miller, A.R., Rutter, E.D., Gurnett, C.A., Vanoye, C.G., George, A.L., Kearney, J.A., 2011. Voltage-gated potassium channel KCNV2 (Kv8.2) contributes to epilepsy susceptibility. Proc. Natl. Acad. Sci. 108, 5443 LP – 5448. https://doi.org/10.1073/pnas.1017539108

Kalmbach, B.E., Johnston, D., Brager, D.H., 2015. Cell-Type Specific Channelopathies in the Prefrontal Cortex of the fmr1-/y Mouse Model of Fragile X Syndrome. eNeuro 2, ENEURO.0114-15.2015. https://doi.org/10.1523/ENEURO.0114-15.2015

Kim, H.W., Quan, Z., Kim, Y.-B., Cheong, E., Kim, H.D., Cho, M., Jang, J., Yoo, Y.R., Lee, J.S., Kim, J.H., Kim, Y.I., Kim, D.-S., Kang, H.-C., 2018. Differential effects on sodium current impairments by distinct SCN1A mutations in GABAergic neurons derived from Dravet syndrome patients. Brain Dev. 40, 287–298. https://doi.org/10.1016/j.braindev.2017.12.002

Landis, B.J., Schubert, J.A., Lai, D., Jegga, A.G., Shikany, A.R., Foroud, T., Ware, S.M., Hinton, R.B., 2017. Exome Sequencing Identifies Candidate Genetic Modifiers of Syndromic and Familial Thoracic Aortic Aneurysm

1162 Severity. J. Cardiovasc. Transl. Res. 10, 423–432.
1163 https://doi.org/10.1007/s12265-017-9753-1
1164 Liang, G., Zhang, Y., 2013. Genetic and epigenetic variations in iPSCs:
1165 potential causes and implications for application. Cell Stem Cell.
1166 https://doi.org/10.1016/j.stem.2013.07.001
1167 Liu, J., Gao, C., Chen, W., Ma, W., Li, X., Shi, Y., Zhang, H., Zhang, L., Long,
1168 Y., Xu, H., Guo, X., Deng, S., Yan, X., Yu, D., Pan, G., Chen, Y., Lai, L.,
1169 Liao, W., Li, Z., 2016. CRISPR/Cas9 facilitates investigation of neural
1170 circuit disease using human iPSCs: mechanism of epilepsy caused by an
1171 SCN1A loss-of-function mutation. Transl Psychiatry 6, e703.
1172 Liu, Y., Lopez-Santiago, L.F., Yuan, Y., Jones, J.M., Zhang, H., O'Malley, H.A.,
1173 Patino, G.A., O'Brien, J.E., Rusconi, R., Gupta, A., Thompson, R.C.,
1174 Natowicz, M.R., Meisler, M.H., Isom, L.L., Parent, J.M., 2013. Dravet
1175 syndrome patient-derived neurons suggest a novel epilepsy mechanism.
1176 Ann. Neurol. 74, 128–139. https://doi.org/10.1002/ana.23897
1177 Lorincz, A., Nusser, Z., 2008. Cell-type-dependent molecular composition of the
1178 axon initial segment. J. Neurosci. 28, 14329–14340.
1179 https://doi.org/10.1523/JNEUROSCI.4833-08.2008
1180 Marian, A.J., 2011. Modeling human disease phenotype in model organisms:
1181 "It's only a model!" Circ. Res. 109, 356–359.
1182 https://doi.org/10.1161/CIRCRESAHA.111.249409
1183 Martin, M.S., Dutt, K., Papale, L.A., Dube, C.M., Dutton, S.B., de Haan, G.,
1184 Shankar, A., Tufik, S., Meisler, M.H., Baram, T.Z., Goldin, A.L., Escayg, A.,
1185 2010. Altered function of the SCN1A voltage-gated sodium channel leads

1186 to gamma-aminobutyric acid-ergic (GABAergic) interneuron abnormalities.
1187 J. Biol. Chem. 285, 9823–9834. https://doi.org/10.1074/jbc.M109.078568
1188 Maxwell, E.K., Schnitzler, C.E., Havlak, P., Putnam, N.H., Nguyen, A.-D.,
1189 Moreland, R.T., Baxevanis, A.D., 2014. Evolutionary profiling reveals the
1190 heterogeneous origins of classes of human disease genes: implications for
1191 modeling disease genetics in animals. BMC Evol. Biol. 14, 212.
1192 https://doi.org/10.1186/s12862-014-0212-1
1193 Meng, H., Xu, H.-Q., Yu, L., Lin, G.-W., He, N., Su, T., Shi, Y.-W., Li, B., Wang,
1194 J., Liu, X.-R., Tang, B., Long, Y.-S., Yi, Y.-H., Liao, W.-P., 2015. The SCN1A
1195 mutation database: updating information and analysis of the relationships
1196 among genotype, functional alteration, and phenotype. Hum. Mutat. 36,
1197 573–580. https://doi.org/10.1002/humu.22782
1198 Miller, I., Sotero de Menezes, M., 2014. SCN1A-Related Seizure Disorders.
1199 University of Washington, Seattle, Seattle.
1200 Mistry, A.M., Thompson, C.H., Miller, A.R., Vanoye, C.G., George, A.L.J.,
1201 Kearney, J.A., 2014. Strain- and age-dependent hippocampal neuron
1202 sodium currents correlate with epilepsy severity in Dravet syndrome mice.
1203 Neurobiol. Dis. 65, 1–11. https://doi.org/10.1016/j.nbd.2014.01.006
1204 Odawara, A., Katoh, H., Matsuda, N., Suzuki, I., 2016. Physiological maturation
1205 and drug responses of human induced pluripotent stem cell-derived
1206 cortical neuronal networks in long-term culture. Sci. Rep. 6, 26181.
1207 Ogiwara, I., Iwasato, T., Miyamoto, H., Iwata, R., Yamagata, T., Mazaki, E.,
1208 Yanagawa, Y., Tamamaki, N., Hensch, T.K., Itohara, S., Yamakawa, K.,
1209 2013. Nav1.1 haploinsufficiency in excitatory neurons ameliorates seizure-

1210 associated sudden death in a mouse model of Dravet syndrome. Hum.
1211 Mol. Genet. 22, 4784–4804. https://doi.org/10.1093/hmg/ddt331
1212 Ogiwara, I., Miyamoto, H., Morita, N., Atapour, N., Mazaki, E., Inoue, I.,
1213 Takeuchi, T., Itohara, S., Yanagawa, Y., Obata, K., Furuichi, T., Hensch,
1214 T.K., Yamakawa, K., 2007. Nav1.1 localizes to axons of parvalbumin-
1215 positive inhibitory interneurons: a circuit basis for epileptic seizures in mice
1216 carrying an Scn1a gene mutation. J. Neurosci. 27, 5903–5914.
1217 https://doi.org/10.1523/JNEUROSCI.5270-06.2007
1218 Ohmori, I., Ouchida, M., Kobayashi, K., Jitsumori, Y., Mori, A., Michiue, H.,
1219 Nishiki, T., Ohtsuka, Y., Matsui, H., 2013. CACNA1A variants may modify
1220 the epileptic phenotype of Dravet syndrome. Neurobiol. Dis. 50, 209–217.
1221 https://doi.org/10.1016/j.nbd.2012.10.016
1222 Ohmori, I., Ouchida, M., Miki, T., Mimaki, N., Kiyonaka, S., Nishiki, T.,
1223 Tomizawa, K., Mori, Y., Matsui, H., 2008. A CACNB4 mutation shows that
1224 altered Ca(v)2.1 function may be a genetic modifier of severe myoclonic
1225 epilepsy in infancy. Neurobiol. Dis. 32, 349–354.
1226 https://doi.org/10.1016/j.nbd.2008.07.017
1227 Paquet, D., Kwart, D., Chen, A., Sproul, A., Jacob, S., Teo, S., Olsen, K.M.,
1228 Gregg, A., Noggle, S., Tessier-Lavigne, M., 2016. Efficient introduction of
1229 specific homozygous and heterozygous mutations using CRISPR/Cas9.
1230 Nature 533, 125–129. https://doi.org/10.1038/nature17664
1231 Parent, J.M., Anderson, S.A., 2015. Reprogramming patient-derived cells to
1232 study the epilepsies. Nat. Neurosci. 18, 360–366.
1233 https://doi.org/10.1038/nn.3944

1234 Rouhani, F., Kumasaka, N., de Brito, M.C., Bradley, A., Vallier, L., Gaffney, D.,
1235 2014. Genetic Background Drives Transcriptional Variation in Human
1236 Induced Pluripotent Stem Cells. PLOS Genet. 10, e1004432.
1237 Rubinstein, M., Han, S., Tai, C., Westenbroek, R.E., Hunker, A., Scheuer, T.,
1238 Catterall, W.A., 2015. Dissecting the phenotypes of Dravet syndrome by
1239 gene deletion. Brain 138, 2219–2233.
1240 https://doi.org/10.1093/brain/awv142
1241 Sandoe, J., Eggan, K., 2013. Opportunities and challenges of pluripotent stem
1242 cell neurodegenerative disease models. Nat Neurosci 16, 780–789.
1243 Scheffer, I.E., Berkovic, S.F., 1997. Generalized epilepsy with febrile seizures
1244 plus. A genetic disorder with heterogeneous clinical phenotypes. Brain
1245 120, 479–490.
1246 Schutte, R.J., Xie, Y., Ng, N.N., Figueroa, P., Pham, A.T., O'Dowd, D.K., 2018.
1247 Astrocyte-enriched feeder layers from cryopreserved cells support
1248 differentiation of spontaneously active networks of human iPSC-derived
1249 neurons. J. Neurosci. Methods 294, 91–101.
1250 https://doi.org/10.1016/j.jneumeth.2017.07.019
1251 Schutte, S.S., Schutte, R.J., Barragan, E. V, O'Dowd, D.K., 2016. Model
1252 systems for studying cellular mechanisms of SCN1A-related epilepsy. J.
1253 Neurophysiol. 115, 1755–1766. https://doi.org/10.1152/jn.00824.2015
1254 Shao, L.-R., Habela, C.W., Stafstrom, C.E., 2019. Pediatric Epilepsy
1255 Mechanisms: Expanding the Paradigm of Excitation/Inhibition Imbalance.
1256 Child. (Basel, Switzerland) 6. https://doi.org/10.3390/children6020023
1257 Singh, N.A., Pappas, C., Dahle, E.J., Claes, L.R.F., Pruess, T.H., De Jonghe,

1258 P., Thompson, J., Dixon, M., Gurnett, C., Peiffer, A., White, H.S., Filloux,
1259 F., Leppert, M.F., 2009. A role of SCN9A in human epilepsies, as a cause
1260 of febrile seizures and as a potential modifier of Dravet syndrome. PLoS
1261 Genet. 5, e1000649. https://doi.org/10.1371/journal.pgen.1000649
1262 Smith, J.G.W., Owen, T., Bhagwan, J.R., Mosqueira, D., Scott, E., Mannhardt,
1263 I., Patel, A., Barriales-Villa, R., Monserrat, L., Hansen, A., Eschenhagen,
1264 T., Harding, S.E., Marston, S., Denning, C., 2018. Isogenic Pairs of hiPSC-
1265 CMs with Hypertrophic Cardiomyopathy/LVNC-Associated ACTC1 E99K
1266 Mutation Unveil Differential Functional Deficits. Stem cell reports 11, 1226–
1267 1243. https://doi.org/10.1016/j.stemcr.2018.10.006
1268 Stover, A.E., Brick, D.J., Nethercott, H.E., Banuelos, M.G., Sun, L., O'Dowd,
1269 D.K., Schwartz, P.H., 2013. Process-based expansion and neural
1270 differentiation of human pluripotent stem cells for transplantation and
1271 disease modeling. J. Neurosci. Res. 91, 1247–1262.
1272 https://doi.org/10.1002/jnr.23245
1273 Stover, A.E., Schwartz, P.H., 2011. Adaptation of Human Pluripotent Stem Cells
1274 to Feeder-Free Conditions in Chemically Defined Medium with Enzymatic
1275 Single-Cell Passaging. Methods Mol. Biol. 767, 137–146.
1276 https://doi.org/10.1007/978-1-61779-201-4_10
1277 Stühmer, W., Methfessel, C., Sakmann, B., Noda, M., Numa, S., 1987. Patch
1278 clamp characterization of sodium channels expressed from rat brain cDNA.
1279 Eur. Biophys. J. 14, 131–138.
1280 Sugawara, T., Tsurubuchi, Y., Agarwala, K.L., Ito, M., Fukuma, G., Mazaki-
1281 Miyazaki, E., Nagafuji, H., Noda, M., Imoto, K., Wada, K., Mitsudome, A.,

Kaneko, S., Montal, M., Nagata, K., Hirose, S., Yamakawa, K., 2001. A missense mutation of the Na+ channel alpha II subunit gene Na(v)1.2 in a patient with febrile and afebrile seizures causes channel dysfunction. Proc. Natl. Acad. Sci. U. S. A. 98, 6384–6389. https://doi.org/10.1073/pnas.111065098

Sun, L., Gilligan, J., Staber, C., Schutte, R.J., Nguyen, V., O'Dowd, D.K., Reenan, R., 2012. A knock-in model of human epilepsy in Drosophila reveals a novel cellular mechanism associated with heat-induced seizure. J. Neurosci. https://doi.org/10.1523/JNEUROSCI.2932-12.2012

Sun, Y., Paşca, S.P., Portmann, T., Goold, C., Worringer, K.A., Guan, W., Chan, K.C., Gai, H., Vogt, D., Chen, Y.-J.J., Mao, R., Chan, K., Rubenstein, J.L.R., Madison, D. V, Hallmayer, J., Froehlich-Santino, W.M., Bernstein, J.A., Dolmetsch, R.E., 2016. A deleterious Nav1.1 mutation selectively impairs telencephalic inhibitory neurons derived from Dravet Syndrome patients. Elife 5, e13073. https://doi.org/10.7554/eLife.13073

Tai, C., Abe, Y., Westenbroek, R.E., Scheuer, T., Catterall, W.A., 2014. Impaired excitability of somatostatin- and parvalbumin-expressing cortical interneurons in a mouse model of Dravet syndrome. Proc. Natl. Acad. Sci. U. S. A. 111, E3139-48. https://doi.org/10.1073/pnas.1411131111

Tidball, A.M., Parent, J.M., 2016. Concise Review: Exciting Cells: Modeling Genetic Epilepsies with Patient-Derived Induced Pluripotent Stem Cells. Stem Cells 34, 27–33. https://doi.org/10.1002/stem.2203

Vitale, A.M., Matigian, N.A., Ravishankar, S., Bellette, B., Wood, S.A., Wolvetang, E.J., Mackay-Sim, A., 2012. Variability in the Generation of

Induced Pluripotent Stem Cells: Importance for Disease Modeling. Stem Cells Transl. Med. https://doi.org/10.5966/sctm.2012-0043

Wallace, R.H., Marini, C., Petrou, S., Harkin, L.A., Bowser, D.N., Panchal, R.G., Williams, D.A., Sutherland, G.R., Mulley, J.C., Scheffer, I.E., Berkovic, S.F., 2001a. Mutant GABA(A) receptor gamma2-subunit in childhood absence epilepsy and febrile seizures. Nat. Genet. 28, 49–52. https://doi.org/10.1038/88259

Wallace, R.H., Scheffer, I.E., Barnett, S., Richards, M., Dibbens, L., Desai, R.R., Lerman-Sagie, T., Lev, D., Mazarib, A., Brand, N., Ben-Zeev, B., Goikhman, I., Singh, R., Kremmidiotis, G., Gardner, A., Sutherland, G.R., George Jr, A.L., Mulley, J.C., Berkovic, S.F., 2001b. Neuronal sodium-channel alpha1-subunit mutations in generalized epilepsy with febrile seizures plus. Am. J. Hum. Genet. 68, 859–865. https://doi.org/10.1086/319516

Wallace, R.H., Scheffer, I.E., Parasivam, G., Barnett, S., Wallace, G.B., Sutherland, G.R., Berkovic, S.F., Mulley, J.C., 2002. Generalized epilepsy with febrile seizures plus: mutation of the sodium channel subunit SCN1B. Neurology 58, 1426–1429.

Wallace, R.H., Wang, D.W., Singh, R., Scheffer, I.E., George, A.L.J., Phillips, H.A., Saar, K., Reis, A., Johnson, E.W., Sutherland, G.R., Berkovic, S.F., Mulley, J.C., 1998. Febrile seizures and generalized epilepsy associated with a mutation in the Na+-channel beta1 subunit gene SCN1B. Nat. Genet. 19, 366–370. https://doi.org/10.1038/1252

Watanabe, E., Fujikawa, A., Matsunaga, H., Yasoshima, Y., Sako, N.,

Yamamoto, T., Saegusa, C., Noda, M., 2000. Nav2/NaG channel is involved in control of salt-intake behavior in the CNS. J. Neurosci. 20, 7743–7751.

Xie, Y., Schutte, R.J., Ng, N.N., Ess, K.C., Schwartz, P.H., O'Dowd, D.K., 2018. Reproducible and efficient generation of functionally active neurons from human hiPSCs for preclinical disease modeling. Stem Cell Res. 26, 84–94. https://doi.org/10.1016/j.scr.2017.12.003

Yu, F.H., Mantegazza, M., Westenbroek, R.E., Robbins, C.A., Kalume, F., Burton, K.A., Spain, W.J., McKnight, G.S., Scheuer, T., Catterall, W.A., 2006. Reduced sodium current in GABAergic interneurons in a mouse model of severe myoclonic epilepsy in infancy. Nat. Neurosci. 9, 1142–1149. https://doi.org/10.1038/nn1754

Yu, J., Vodyanik, M.A., Smuga-Otto, K., Antosiewicz-Bourget, J., Frane, J.L., Tian, S., Nie, J., Jonsdottir, G.A., Ruotti, V., Stewart, R., Slukvin, I.I., Thomson, J.A., 2007. Induced pluripotent stem cell lines derived from human somatic cells. Science 318, 1917–1920. https://doi.org/10.1126/science.1151526